AD-A283 957

Dist: A

TION PAGE

Form Approved
OMB No. 0704-0188

1. AGENCY USE ONLY (Leave blank)	2. REPORT DATE	3. REPORT TYPE AND DATES COVERED
	June 15, 1994	Final, April 1, 1992-Jan 14, 1994

4. TITLE AND SUBTITLE

Interface Mechanics of Particulate Media with Ribbed Inclusions

5. FUNDING NUMBERS

F49620-92-J-0216

2302/CS

6. AUTHOR(S)

Roman D. Hryciw
Scott A. Raschke
Masyhur Irsyam

7. PERFORMING ORGANIZATION NAME(S) AND ADDRESS(ES)

The University of Michigan
DRDA, Wolverine Tower
3003 S. State St.
Ann Arbor, MI 48104

8. PERFORMING ORGANIZATION REPORT NUMBER

UMCEE 94-19

AFOSR-TR- 94 0478

9. SPONSORING/MONITORING AGENCY NAME(S) AND ADDRESS(ES)

AFOSR
Building 410
Bolling AFB, DC 20332-6448

NA

10. SPONSORING/MONITORING AGENCY REPORT NUMBER

~~AFOSR~~ F49620-92-J-0216

11. SUPPLEMENTARY NOTES

12a. DISTRIBUTION/AVAILABILITY STATEMENT

Approved for public release, distribution unlimited

A

12b. DISTRIBUTION CODE

13. ABSTRACT *(Maximum 200 words)*

A large half-axisymmetric triaxial apparatus for studying the pullout resistance and interface mechanics of cylindrical ribbed inclusions in particulate material (soil) was designed, constructed and tested. The unusual geometry was needed to facilitate visual observation of grain motions, the changing soil fabric and shear band development around the inclusions. Initially, it will provide verification of a previously developed plasticity model for soil-ribbed inclusion interaction. The model is based on the development of passive soil resistance to advancing ribs in a plane strain geometry. The results of these plane strain observations are presented. While the model has been theoretically extended to cylindrical inclusions, experimental verification, including the observation of soil grain behavior in the vicinity of ribs, has hitherto not been conducted.

Computer visualization hardware and software for tracking the displacements and rotations of individual particles has been developed. The system includes a computer workstation, a laser video disk recorder and digitizing boards. The software was written at the University of New Mexico and modified for the testing program at the University of Michigan. A CCD video camera and bellows system allow for 1:10 to 5:1 magnifications. Various combinations of opaque dyes and color filters optimize the visual data collection while computer enhancement prepares the data for edge detection and particle tracking.

14. SUBJECT TERMS	15. NUMBER OF PAGES
Particulate media, computer vision, experimental micromechanics	37
	16. PRICE CODE

17. SECURITY CLASSIFICATION OF REPORT	18. SECURITY CLASSIFICATION OF THIS PAGE	19. SECURITY CLASSIFICATION OF ABSTRACT	20. LIMITATION OF ABSTRACT
unclassified	unclassified	unclassified	UL

TABLE OF CONTENTS

1.0 PROJECT OBJECTIVES

The objectives of this study included:

a) Reduction and analysis of previously collected data on interface mechanics of plane ribbed inclusions in particulate matter;

b) Development of a computer visualization system to assist in the study of soil micro-kinetics and micromechanics.

c) Construction of a large 1/2-axisymmetric triaxial apparatus for testing interface mechanics of cylindrical ribbed inclusions in particulate matter;

2.0 STATUS OF RESEARCH EFFORT

a) The plane strain data has been analyzed. The results of this work have been documented in a paper published in Soils and Foundations, the Journal of the Japanese Society of Soil Mechanics and Foundation Engineering. A copy of the paper is included as an appendix to this report.

b). The computer visualization system was assembled at the University of New Mexico by Dr. Gregory Donohoe of the Electrical and Computer Engineering Department and was delivered to the University of Michigan late in 1993. Hardware problems developed in January of 1994, shortly after receipt of the system from New Mexico. The result has been a delay of approximately 6 months while waiting for replacement components. It is anticipated that the visualization system will be operational by July, 1994.

c) Construction of the large 1/2-axisymmetric triaxial apparatus has been completed with some additional modifications from the original design. These include: the addition of strain gauges along the lengths of the inclusions in order to directly measure load transfer along a single "rib spacing" and the deletion of carbo-wax impregnation methods from the test program. The latter change may be reversed if a need arises. Several pilot tests have now been conducted and minor adjustments are being made to the testing procedure prior to implementation of the computer visualization system.

3.0 BEHAVIOR OF SAND PARTICLES AROUND RIGID RIBBED INCLUSIONS DURING SHEAR

An experimental investigation of the behavior of sand particles around rigid ribbed inclusions was performed. The results of these investigations have been documented by Hryciw and Irsyam (1993) which is included as Appendix A to this report. A brief synopsis of methods and findings are presented here:

Direct shear tests were conducted in a large plexiglass-walled shear device. This allowed the movements of individual sand grains to be followed during shear. Zones of relatively high contraction, dilation and shear strain increment around rigid ribbed inclusions were mapped. In dense sand, dilation, followed by progressive formation of a

shear surface was observed and related to the development of peak and residual strengths. In loose sands, contraction was clearly in evidence and no peak behavior was discerned. Upon reversal of the shearin ection, and on all subsequent shearing cycles, both initially dense and loose san played similar behavior and similar shearing resistance thereby confirming the establishment of a critical void ratio.

Carbowax solidification techniques (Hryciw and Irsyam, 1990) were used to determine the shapes of the shear surfaces and to establish the void ratios in the intrarib region. In general, there was excellent agreement between the carbowax test results and visual observations.

Tests were also conducted to investigate the effects of rib spacing, rib geometry, grain size and grain shape. While full passive zones developed for a relatively large rib spacing of 33 mm, at a 25.2 mm spacing grains were trapped between the ribs and only a partial passive zone could develop. Previous studi syam and Hryciw, 1991) have shown that the pullout resistance is highest when the nu ull passive zones per length of inclusion is maximized.

Small, closely spaced trapezoidal ribs such as found on reinforcing rods were incapable of producing a passive zone. However, a shear zone was observed to develop through the sand above the ribs. By contrast, no shear zone whatsoever was observed for smooth plates. The grains essentially slipped along the rib-less surface during shear.

Angular sands displayed greater movement than rounded sands prior to residual strength development and the passive zone was generally larger. Ottawa 20-30 and Ottawa 40-50 sands displayed very similar behavior. Full details of this experimental program and results are found in Appendix A.

4.0 DEVELOPMENT OF COMPUTER PARTICLE TRACKING SYSTEM

4.1 Introduction

The particle tracking system is used to track and map the motion of individual grains in a particulate assembly (soil) subjected to a stress field. This allows the trajectories of particles to be quickly and accurately established under various boundary and soil conditions in real time. The particle tracking system consists of both hardware and software components as described below.

4.2. Hardware Description

The particle tracking system, shown schematically in Figures 1 and 2, is centered around a Sun Sparcstation 2 computer (a Sun 4 computer) running SunOS 4.1.3, X11R5, and OSF Motif 1.2.2. The computer has 32 MB RAM memory, two 424 MB hard disks for data storage and disk caching, and a 19 inch color monitor. The Sun Sparcstation is the primary component of the tracking system. It acts as the primary user interface to the system and controls the peripheral devices. It is used for data analysis using the particle tracker software and for data visualization using Khoros. The Sparcstation is networked on the University of Michigan's Computer Aided Engineering Network (CAEN), which

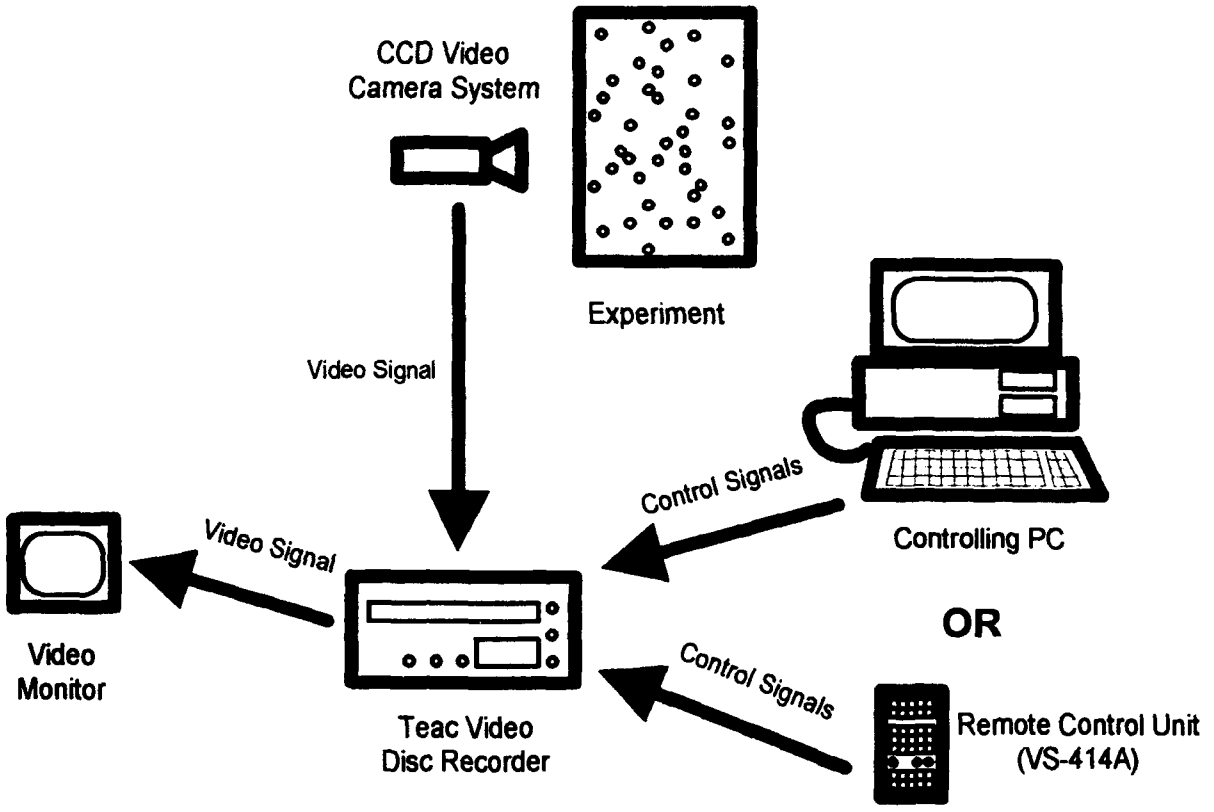

Fig. 1. Visual data collection system.

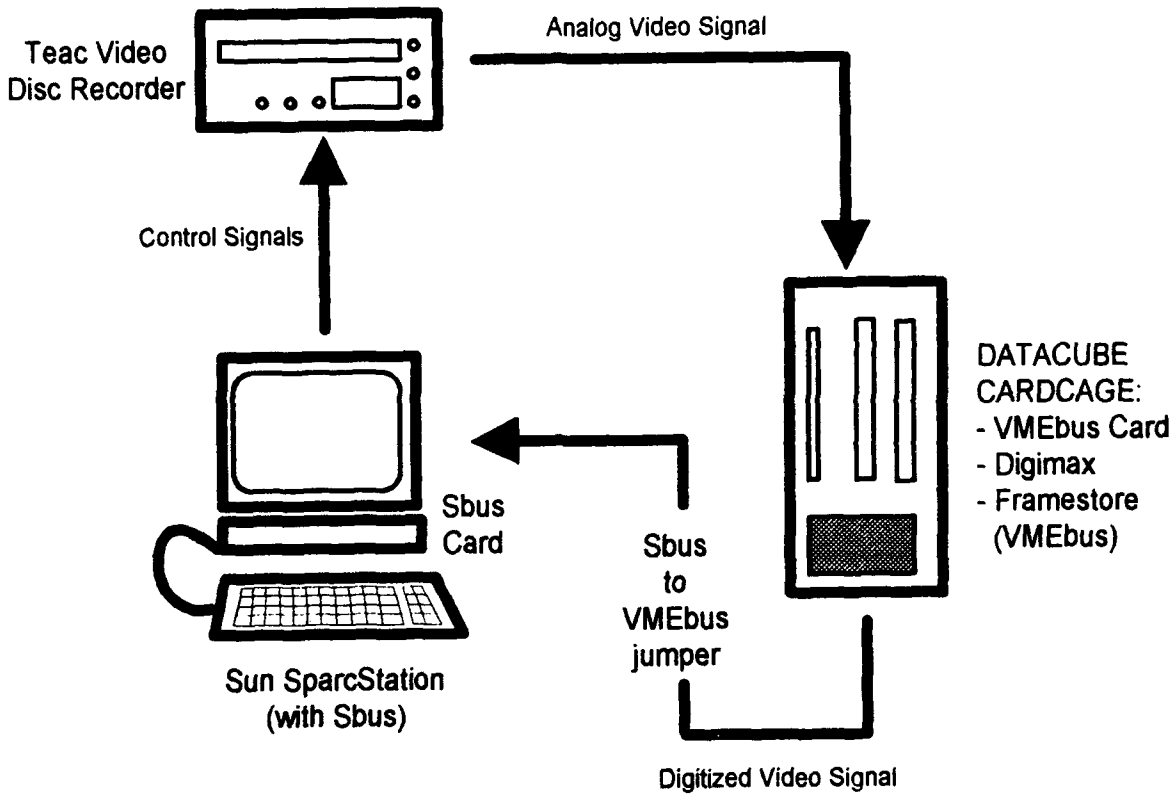

Fig. 2. Data analysis system.

allows it access to additional software. The other peripheral hardware accessories used to capture and store images and data are listed as follows:

1. Laser video disc recorder (VDR)
2. Video processing modules
    a. Digitizer
    b. Framebuffer
3. Sbus-to-VMEbus adapter
    a. Sbus card
    b. VMEbus card
    c. VMEbus cardcage with power supply
4. CCD video camera system
    a. Macro lens (FD 50mm f/3.5)
    b. Extension tube (FD 25-U)
    c. Bellows R
    d. Polarizing and color filters
    e. Ring lighting system
5. B/W video monitor (9 inch)

A description of these system components and their functions follow:

4.2.1. Laser Video Disc Recorder

The Teac LV-210A, shown in Figures 1 and 2, is a laser video disc recorder capable of recording and playing back an NTSC video signal and two channels of audio. It can be controlled by a wireless remote control unit (VS-414A) or a personal computer over a serial cable using an RS-232C interface. The video disc recorder allows video sequences to be recorded a single frame at a time, continuously, or using time-lapse recording at any desired frame rate. Custom programs including combinations of one-frame recording, continuous recording or interval recording as well as multi-speed playback are available. The disk recorder writes to an optical memory disc, which is not erasable. This type of storage unit is often referred to as a WORM (write once read many) disc. Each disc may store 60 minutes of video and stereo audio (30 minutes each side) or 108,000 frames of still pictures and compressed still-frame audio (54,000 frames per side). Since 515x512 gray-scale byte (8 bit) images occupy approximately 250,000 bytes, this translates into about 27 Gigabytes (27,000 MB) of image data storage, which makes it ideal for archival purposes of image data. WORM discs also have a shelf life of over 30 years without any special environmental storage requirements (Gonzalez and Woods, 1992). Once a sequence of images is recorded, individual images can be recalled to the computer (under computer control) for analysis. Images stored on the Teac VDR are much more stable and with higher resolution than if they were stored on other media such as video cassette recorder (VCR) tapes.

4.2.2. Video Processing Modules

The "Digimax" and "Framestore" shown in Figure 2 are the digitizing and framebuffer cards, respectively, produced by Datacube as part of their MaxVideo line. These modules are contained in a "VMEbus cardcage" and are the interface between the analog images recorded on the optical discs and the Sun Sparcstation. The Digimax video digitizer performs an A/D conversion on an incoming image from the Teac VDR. It features computer adjustable video gain and offset, graphical overlays on output and switchable inputs. Once an image has been digitized, it is sent to the Framestore module and held in a memory buffer until the computer is ready to accept the image. The operation of the Framestore module is tightly coupled with the Digimax. There is a video output connection from the Digimax which may be connected to the video monitor to display the current contents of the Framestore image memory.

4.2.3. S bus-to-VMEbus Adapter

The Datacube MaxVideo modules discussed above operate using a VMEbus which is incompatible with the Sbus in the Sun 4. In order to transfer image data and commands between the Sun 4 and the Datacube hardware, an Sbus-to-VMEbus adapter (PT-SBS915) is used. The adapter consists of two cards. The Sbus card is installed in the Sparcstation and the VMEbus card is installed in the VMEbus cardcage with the MaxVideo modules.

4.2.4. CCD Video Camera System

The Pulnix TM-7CN is a high-resolution (768H x 494V) CCD video camera which utilizes a ½" interline transfer CCD imager. The camera is equipped with an automatic gain control (AGC) sensor and has excellent low-light sensitivity (1 lux). The Canon FD 50mm f/3.5 macro lens is specially designed for close-up photography. The lens is specially corrected for aberrations which usually occur at close shooting distances. It provides high resolution and contrast. The fact that the CCD imager is smaller than the 35 mm film format means that the image formed on the imager is much larger than the CCD imager itself. Only the center portion of the lens is therefore used to form the image on the CCD imager. This results in less distortion at high magnifications since image quality is highest at the center, while deteriorating toward the edges. An extension tube and bellows (Figure 3) are used to increase the magnification power of the camera by moving the lens away from the focal plane of the camera. This provides flexibility for obtaining images over a range of magnifications. Magnifications on the order of 1:10 to 5:1 are possible with this configuration.

A ring-light system consists of a 7 inch diameter circular fluorescent light supported by a clamping ring stand. This type of lighting provides diffuse, uniform illumination which minimizes adverse shadowing. Glare and shadowing are two major problems in this application as they cause errors in image analysis, such as in delineating the boundaries of individual particles for segmentation. Improving image quality during acquisition reduces the amount of time required for image processing.

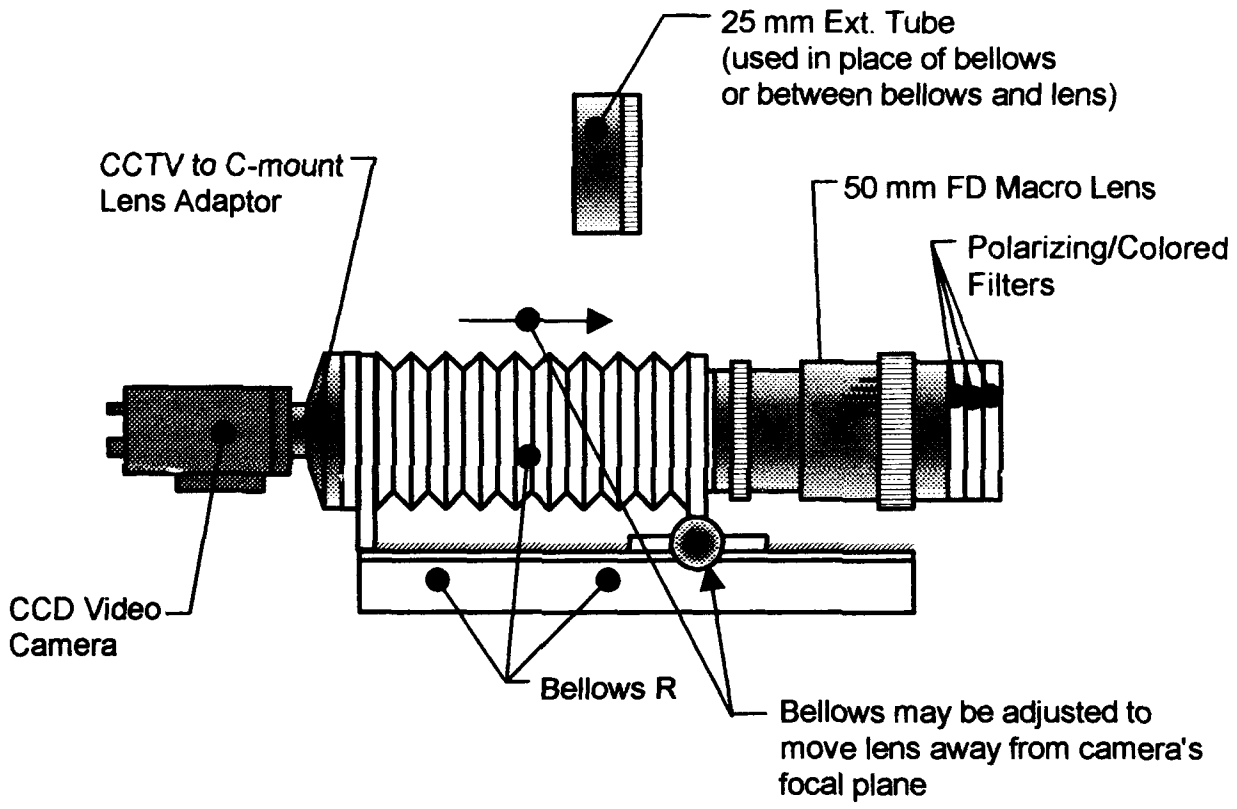

Fig. 3. Video camera system detail.

The Canon lens can be stacked with multiple filters. Two polarizing filters and an assortment of colored filters (red, green, blue, and yellow) are used to improve image quality. Particles assemblies are viewed through a synthetic sapphire window which is built into the walls of the testing apparatus (Section 5.2). The sapphire window produces glare through reflected light. A single linear polarizing filter is therefore used to reduce this glare. Two such polarizing filters both reduce the glare and control the amount of light reaching the camera.

The colored filters aid image analysis by improving the quality of images where there is poor contrast in the particle field. The particle tracker software (Section 4.4) segments particles by creating an edge-map using an edge detection algorithm. The edge detection scheme looks for edges in an image based on changes in its gray-scale value. The Ottawa sand used in this research is composed of quartz particles (which are uniform in color and somewhat translucent); hence, the edge detection scheme would only work based on gray-scale changes due to shadowing along the particle edges. An opaque dye was thus used to create colored Ottawa sand particles. These grains were mixed with naturally colored Ottawa sand so there would be more difference in gray-scale values of the particles. This enhances the contrast in the image to improve the performance of the edge detection scheme. At times, however, the density of colored particles in the image region being recorded is too great. To "eliminate" some of the colored particles from the image, a colored lens is used. A colored filter placed in front of the lens will pass more light of its own color, and block the light of other colors. For instance, using a red filter will cause the red particles to be washed out and appear very similar to the natural Ottawa sand.

4.3 Particle Tracker System Setup

The configuration of the particle tracker system depends on the function it is performing. The system has three basic purposes: data collection, data analysis, and data visualization. Figure 1 shows the equipment configuration for data collection. The entire system is mobile and may be transported to the experiment site. The Teac VDR is used to record an experiment and is controlled with either the wireless remote control unit (VS-414A) or a personal computer (which may be any IBM compatible PC/XT/AT, etc.). Software (written in ANSI C) has been developed to allow the user to control all of the Teac VDR functions from a PC; however, all of these functions are just as easily controlled using the wireless remote. Either option allows the user to control the signal to begin recording, frame-rate, etc. Since it is much more compact than a PC, the wireless remote is generally preferred, especially when the equipment must be transported to an experiment site. Once the experiment is started, images from the video camera are recorded on the VDR. A video monitor wired to the VDR allows the user to see the command menu used to control the VDR and view the experiment as it is being recorded.

Once the experiment has been recorded, the hardware is re-configured as shown in Figure 2 for data analysis. The workstation controls the video disc using software developed at the University of New Mexico called "The Particle Tracker" or "Tracker" for short (Tran, 1993; Donohoe, 1992). The program initializes the VDR and allows the user to select a desired sequence of images from an area on the disc. The selected images are

transferred to the MaxVideo modules (Digimax and Framestore) a single frame at a time. The system selects the first image in the sequence and freezes the image on the VDR. The computer signals the Digimax video digitizing card to convert the selected video frame to a digital image, which is stored temporarily in the Framestore image memory card. The analysis program transfers the digital image over the Sbus to VMEbus jumper to the memory of the Sun. The user can then select the particles to be tracked in succeeding frames. The program calculates the coordinates of the centroid of the projected area of particles as well as their major and minor axes. This information is written to a data file and gives the user the option to save the image of the selected particles as an image file (VIFF format). The user then tells the program to track the selected particles. The program signals the VDR to proceed to digitize the next image frame. The new position and orientation of the previously selected particles in this frame are then determined. The data is recorded and the process continues until all of the frames are analyzed.

4.4 Software Description

The Particle Tracker software was developed at the University of New Mexico as part of this project. The details of the program and its development are found elsewhere (Tran, 1993) but its fundamental operation is outlined here.

Tracker is a stand alone application developed under Khoros. Khoros is an open software product which is used for information processing (primarily image processing) and data visualization under a visual programming environment. It is also a software development tool which can be used to create stand-alone applications such as Tracker. The Khoros environment makes it easier to develop certain parts of the software (e.g., the graphical user interface which is built employing the MIT Athena widget set). Also, programmers can incorporate existing Khoros modules into their software, as well develop their own.

The user interface to the Particle Tracker is shown in Figure 4. Once the program is started, the user interacts with it using a mouse and the keyboard. He/she may select from four main program functions using buttons which bring down individual menus to control the various features in Tracker: File I/O, Track Grains, Video Disc, and Edge Detection.

Functions under the File I/O menu allows the user to select input files from either the VDR or images previously s ed on the computer hard disk. Output filenames for image and data files may also be specified. The Track Grains menu allows a user to begin the tracking process after selecting particles as well as pausing and stopping the tracking process. The Video Disc menu provides access to most of the VDR control functions (e.g., initialize a video disc, play forward, reverse, etc.). The Edge Detection menu allows the user to control parameters used for edge detection, including dynamic threshold value and the minimum length of an edge.

Once a gray-scale image is read into the computer memory, the image is "preprocessed" using a median filter to reduce noise. This stage of the image processing routine increases the chance of successful image analysis. The image is subsequently

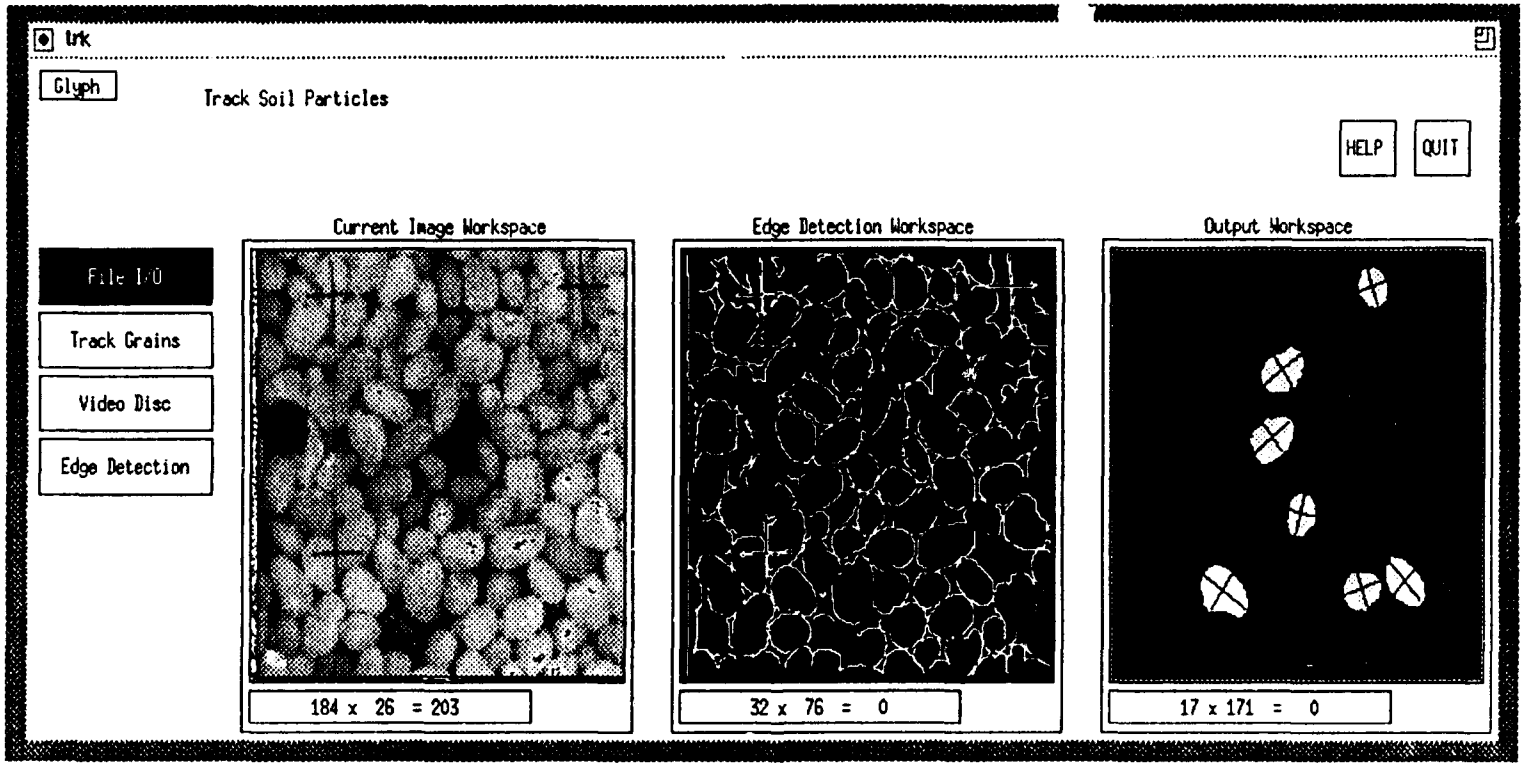

Fig. 4. Graphical user interface for the particle tracker software.

displayed in the first of three "sub-panes" in the main tracker window or pane (see Figure 4). An edge-map image is shown in the second pane. The user selects the particles on the edge-map to be tracked by clicking on them with the mouse. The selected particles are displayed in the output workspace in the third pane. The user then instructs the program to begin tracking. The next image is read from the VDR and digitized. The median filter is applied to this image, it performs the edge detection, completes the boundaries of the selected particles, fills them with foreground pixels, updates their areas, centroid, and orientation. A new edge-map image and output image containing only the selected particles are brought up in two new windows. The location of the centroids, and the orientation of the particles are written to a data file (see Table 1). The output image may also be stored if specified in the File I/O menu. This process is repeated for the entire image sequence or until the user instructs the tracking process to be stopped or paused using the Track Grains menu.

5.0 THE AXISYMMETRIC HALF-TRIAXIAL APPARATUS AND PRELIMINARY RESULTS

5.1 Introduction

Previous research at the University of Michigan sponsored by the AFOSR has led to the development of an analytical model for the pullout resistance of a planar ribbed inclusion in cohesionless soil. This model was extended to the axisymmetric case, however, construction of a new axisymmetric, half-triaxial testing (AHT) device was necessary to verify the solution.

5.2 Description

Development of the axisymmetric, half-triaxial testing apparatus included not only the cell itself, but also supporting equipment including an air-pressure manifold system to regulate cell pressure in the AHT device, a computer controlled hydraulic actuator system for inclusion pullout, electronic data acquisition hardware and software, as well as preparation of two model axisymmetric inclusions: one with and one without ribs.

The AHT cell is shown schematically in Figure 5. The cell consists of a semi-cylindrical steel section fixed between two aluminum end-plates with six threaded bars. Two L-Channel sections were welded along the sides of the semi-cylinder to provide a means for attaching the aluminum top-plate. The top-plate is attached to the end-plates and semi-cylinder with 24 hex bolts as shown in Figure 5. The top plate has two access slots along the centerline and a 4.5 inch hole for a synthetic sapphire viewing window. The hole is larger on the bottom of the top plate (inside the cell) than on the top to form a rim on which the window rests and is cut so it sits flush with the inside surface of the top plate. A 0.5 inch radius semi-circular opening was made in each of the end-plates for the inclusion to pass through. Semi-circular Teflon™ "wipers" are attached inside the openings in the end plates to reduce friction between the bar and the end-plates and to keep soil from escaping out the hole as the inclusion is displaced.

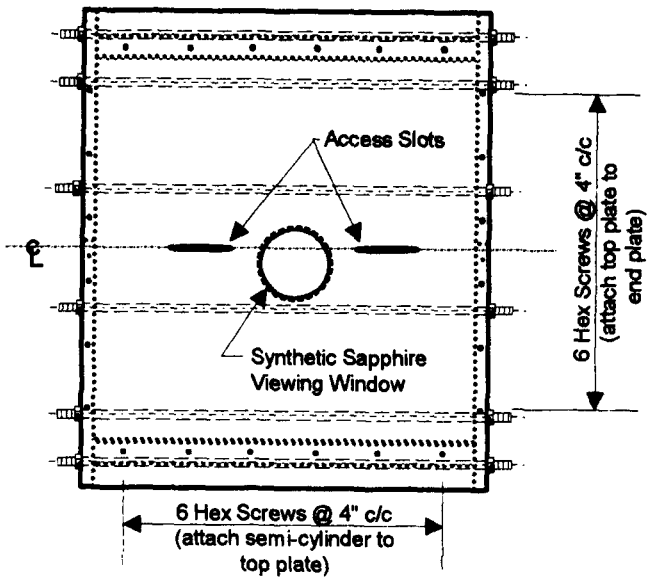

(a) - TOP VIEW

(d) - ORTHOGONAL VIEW

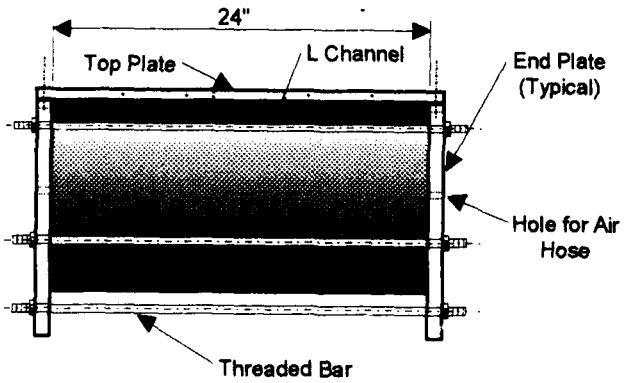

(b) - SIDE VIEW

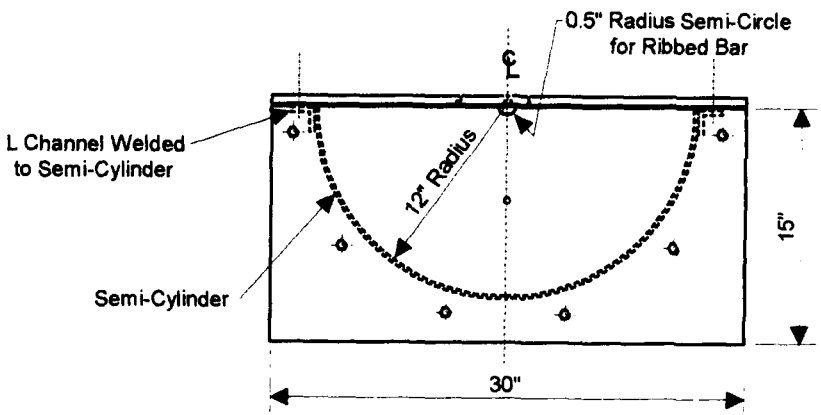

(c) - END VIEW

Fig. 5. Axisymmetric, half-triaxial (AHT) apparatus.

Three rubber bladders are used to control the confining stress in the cell. Two bladders line the ends of the device to control axial stress in the cell, while another bladder along the circumference of the interior of the semi-circular section controls radial stress. Each of the rubber bladders has an individual valve stem. A hole was made in the end plates and the semi-cylindrical steel section to allow access to the valve stems.

A manifold system was constructed to control the pressure in each of the bladders (see Figure 5(d)). The manifold system connects to a 100 psi "house" air pressure supply. The house pressure supply is split to three independent regulators which supply local cell pressure to each of the three bladders. Since each of the bladders can be controlled independently, K_o, or any other biaxial stress conditions, may be simulated.

The AHT cell is centered on a 62 inch long by 32 inch wide steel plate. The cell is restrained laterally and attached to the plate with two steel braces on each end which are bolted to the base plate and AHT cell as shown in Figure 5(d). This entire assembly is welded at the end of a 96 inch long I-Beam.

A closed-loop servo-controlled hydraulic actuator is used to load the inclusion. The actuator is attached to the steel I-Beam as shown in Figure 6. The actuator is an MTS Model 244.22 double-acting, double-ended hydraulic actuator. The actuator has a displacement stroke of 6.6 inches and a capacity of 22 Kips. The hydraulic actuator is powered by a central pump which supplies a nominal working pressure of 5000 psi.

The actuator is controlled using an 406.11 MTS controller. This device allows the actuator to be positioned manually using a set-point dial and will accept an analog input signal through a coaxial cable connection. The actuator has an internal LVDT which is used for closed-loop feedback control. An IBM PC equipped with a Tecmar Lab Master digital-to-analog (D/A) converter card is used to control the loading of the inclusion via the analog input on the controller. A computer program written in BASIC provides a linearly-ramped output voltage to the D/A card which passes the analog voltage to the MTS controller. This allows tests to be performed at a constant rate of displacement. The program allows the user to control the following independent test parameters:

- initial direction of loading (tension or compression)
- number of loading cycles
- displacement rate
- total displacement

As mentioned previously, two inclusions were machined from aluminum bars. The ribbed bar is shown in Figure 7. The radius of the bar is 0.5 inch with a rib spacing of 1.3 inches. This rib spacing results in a fully formed passive zone when sheared through Ottawa 20-30 sand (Irsyam, 1991). Four 350 ohm strain gauges were bonded to the back of the ribbed bar in the groove as shown in Figure 7, so the load take-out within the ribbed region could be measured. A smooth bar with no ribs was made which is otherwise geometrically identical to the ribbed bar. This bar is used to measure friction between the soil and aluminum in the absence of any passive resistance. The inclusions are connected to the actuator piston using a shear pin connection (see Figure 8). An aluminum collar was machined from a solid aluminum rod with one end which could be threaded onto the hydraulic actuator piston and the other end hollowed out so that it fit over the end of the

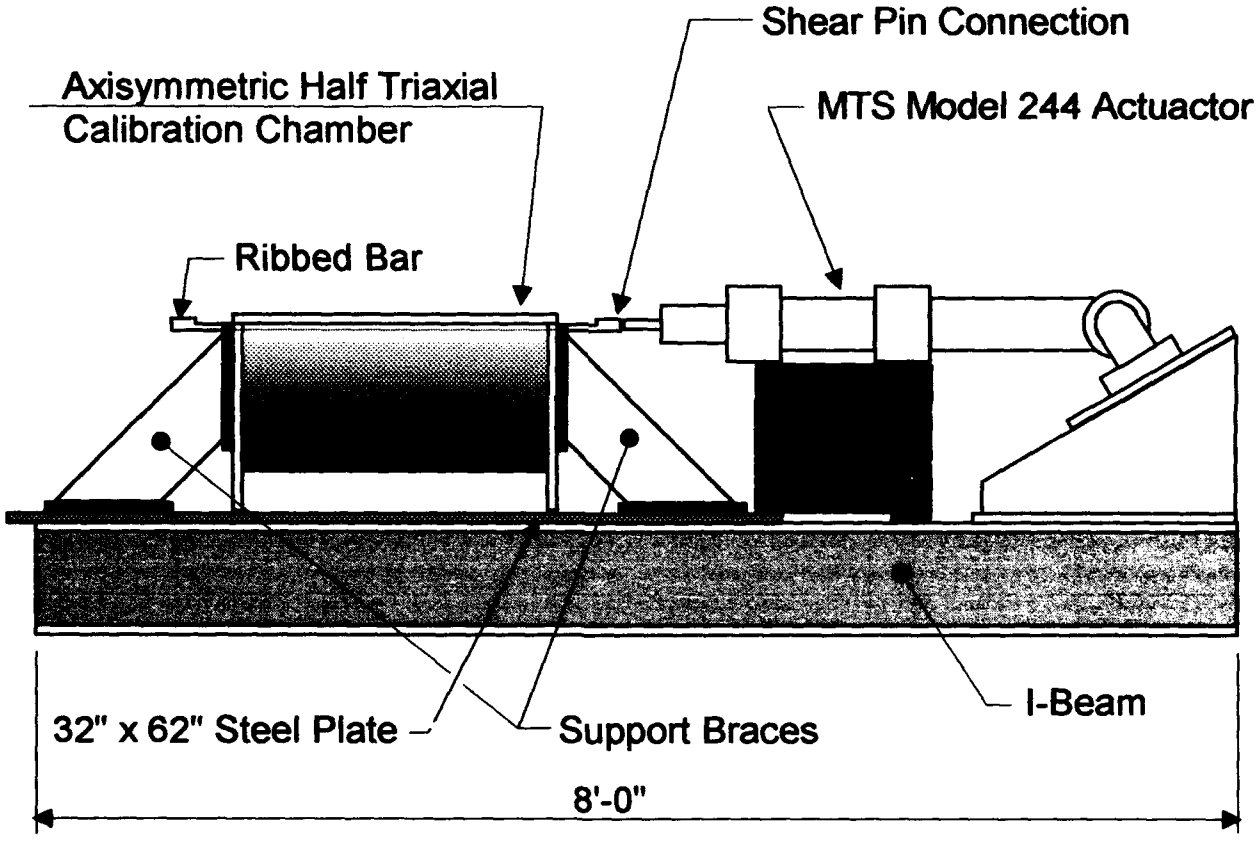

Fig. 6. Loading system for axisymmetric, half-triaxial (AHT) apparatus (drawing to scale).

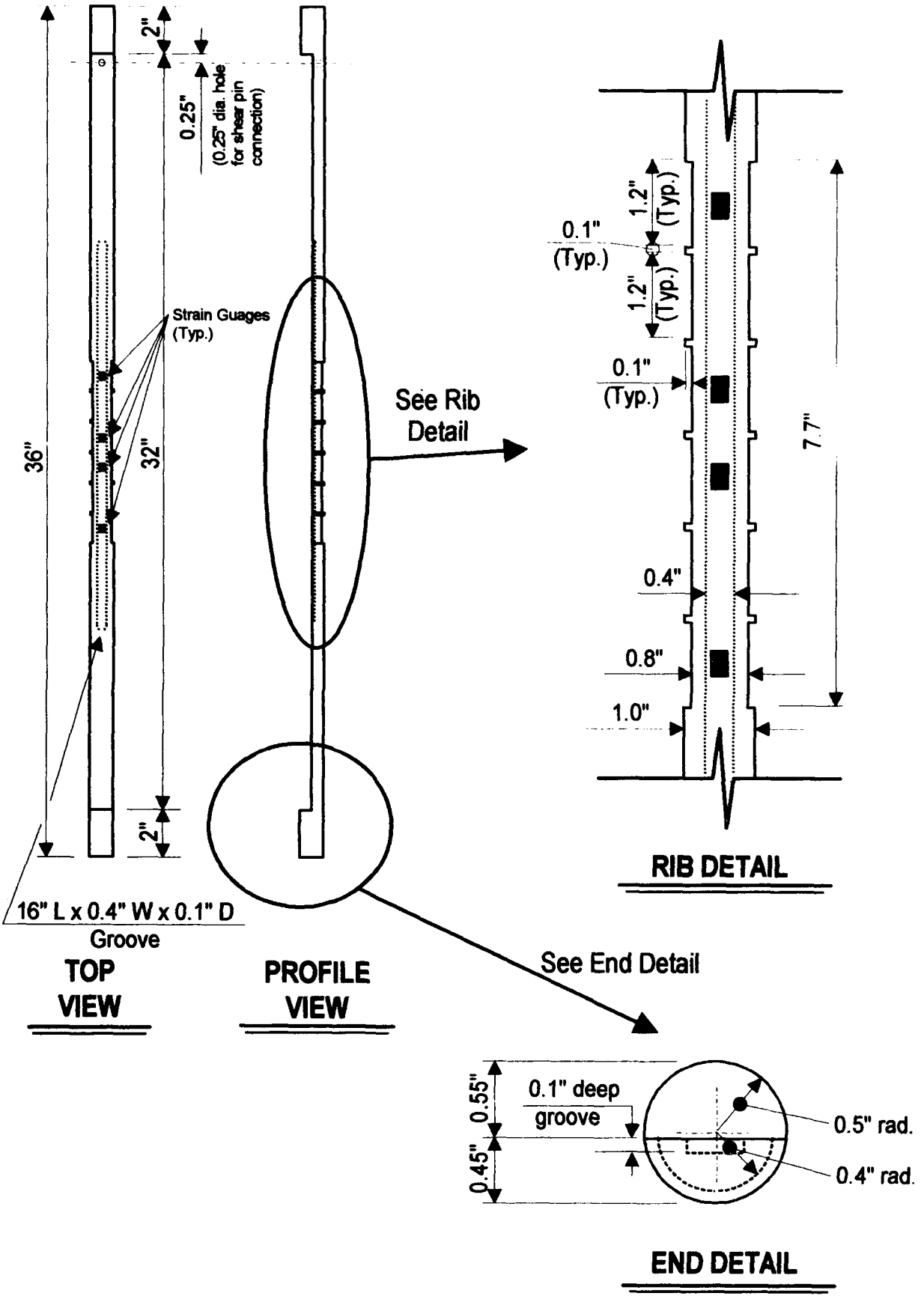

Fig. 7. Axisymmetric ribbed bar used for pullout tests.

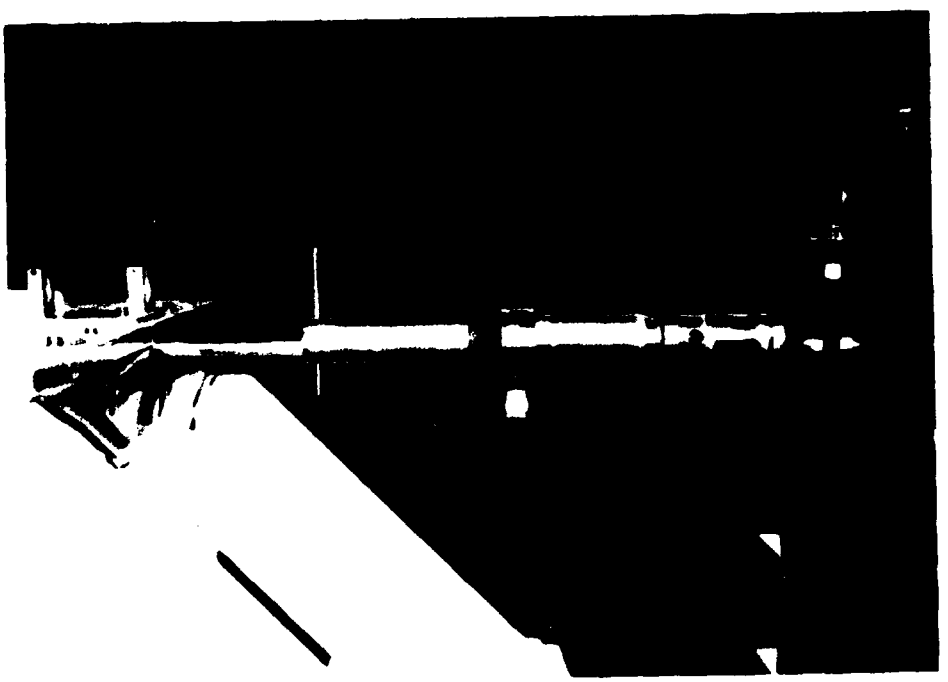

Fig. 8. Shear pin connection.

inclusion. Both the bar and the shear collar have matching holes drilled vertically in them so that they were concentrically aligned. These holes are aligned prior to testing and the bar is attached to the collar with a shear pin.

Data from the tests is collected using a Daytronic System 10 Data Acquisition System which is controlled by a PC microcomputer. This system allows measurements to be made from load cells, LVDTs, and analog voltages from 10 ± volts. A 5 Kip Sensotec load cell is used to measure the total pullout resistance of the bar during loading. The load cell is mounted in between the shear pin connector and the tip of the actuator piston as shown in Figure 8. The displacement of the inclusion during testing is recorded using an LVDT mounted to the top plate of the AHT chamber.

The four strain gauges attached to the ribbed bar are wired into four independent Wheatstone bridge completion circuits. An Analog Devices signal conditioning system is used to condition the signal from the gauges. Four 3B16-01 strain gauge conditioning modules provide a 10 volt excitation voltage to each of the completion bridges. The analog output from the modules are recorded by the Daytronic Data Acquisition System through an 8 channel A/D card. The strain gauges were directly calibrated in terms of load by dead-loading the ribbed bar. Several initial loading cycles were performed prior to calibration to allow the strain gauges to seat adequately.

5.3 Test Procedure

Performing a cyclic loading test involves the following steps:

1. Initializing the computer program which controls the actuator,
2. Selecting the program input parameters, including displacement rate, total displacement and number of loading cycles,
3. Preparing the soil at the desired density in the AHT cell,
4. Placing the top plate on the AHT and securing it with hex-screws,
5. Aligning a shear pin collar with a hole in the inclusion and inserting the pin,
6. Securing an LVDT for measuring inclusion displacement,
7. Initializing the data acquisition system,
8. Applying cell pressure with regulators on a manifold (this is done by simultaneously increasing the axial and radial bladder pressures incrementally by 1 psi until the desired pressure is reached)
9. Starting the data acquisition system and initiating inclusion displacement.

Most of these steps are straightforward with the exception of the placement of the soil and ribbed bar. There are two different techniques which can be used to place the rib in the soil. Each of these methods has its inherent drawbacks and will produce somewhat different results. In the first method, the bar is initially attached to the top plate of the AHT device by screws which pass through the access slots in the top plate and thread into two holes in the back of the ribbed bar. The sapphire window is held in position between the top plate and the bar. After the soil has been placed in the cell at the desired initial density, and scored across the top to level the soil, the top plate (with the ribbed bar attached) is positioned and attached using the hex screws as shown in Figure 1. The screws attaching the ribbed bar to the top plate are then removed.

The drawback to this technique is that pressing the ribbed bar into the soil will compress the soil around the bar. This will alter the void ratio and the soil stress conditions in the vicinity of the bar. The attractiveness of this method is that it realistically simulates the cavity expansion due to installation. Typically, ribbed inclusions (such as re-bar) used in anchored geosynthetic systems are driven or vibrated into the soil. Hence, the soil is displaced radially outward (and downward) as the inclusion is driven which leads to higher densities around the rib. This situation is advantageous for real applications, since higher densities will create larger pullout resistance's.

While the first method may realistically model in-situ installation, it makes it difficult to verify pullout resistance models from experimental data since the void ratio and stress states in the vicinity of the inclusion are unknown. An alternative method consists of placing the inclusion on the openings in the end plates prior to soil preparation. The soil will conform to the shape of the bar and the void ratio around the bar should be typical of the average void ratio of the entire sample. The void ratio is known and can then be used as an independent variable in the pullout resistance models and there will be no increase in radial stress due to cavity expansion.

A final issue which must also be addressed is the friction between the flat portion of the inclusion which is in contact with the top plate. It was anticipated that the interface friction between the inclusion and the top plate could contribute significantly to the pullout load, and would need to be known fairly accurately. It was also necessary to obtain a surface finish which would not change over the course of the testing program due to wear. Both surfaces were wet-sanded in stages with successively finer grades of sand paper. The surface of the top plate was then finished with Sprayon™ Dry Graphite Lube. It was found that this material yields a surface with long-wearing lubrication. Using the lubrication instead of the bear metal-metal contact meant that increased friction due to surface wear was minimized.

In order to account for the friction between the top-plate and inclusion, the interface friction angle or coefficient of friction was determined. Two aluminum blocks were prepared by using the identical finishing technique, followed by application of the graphite lube to one of them. The two blocks were then tested in direct shear at the same range of confining stresses to be used in the pullout tests (5, 10, 15, 20, and 25 psi). The friction angle was determined to be 8.6° ($\mu = 0.15$). Once the friction angle was known, the pullout resistance due to friction between the top-plate and the inclusion can be found as a function of the confining stress through:

$$\frac{P_f}{L} = 2R\sigma_r \tan\delta_f \qquad (1)$$

where,

P_f/L	=	pullout resistance per unit length of inclusion
R	=	radius of the inclusion
σ_r	=	radial confining stress
δ_f	=	interface friction angle between the top plate and the inclusion

5.4 Preliminary Results

The addition of the computer visualization system to the scope of the study precluded an extensive testing program during this funding period, however, preliminary pilot tests were performed. These results are only presented to illustrate that the equipment was working satisfactorily. Several preliminary tests were performed, two of which are presented here. In each case, the bar was placed as outlined in method one (Section 5.3). Figure 9 shows the load-displacement results for the smooth inclusion at a confining stress of 10 psi in loose Ottawa sand ($e \approx 0.69$). The initial loading placed the bar in tension (pullout) and the direction of loading was reversed after a displacement of approximately 1.5 inches. The inclusion was cycled through four loading sequences. Figure 10 shows the load-displacement results for the ribbed inclusion at a confining stress of 10 psi also in loose Ottawa sand ($e \approx 0.69$). Again, the bar was initially pulled-out, and then the direction of loading reversed after about 1.5 inches. A total of two loading cycles were used. The data shown, however, are for a "staged test" in which a loading sequence was performed at a lower confining stress prior to the test for which the results are shown. This is the reason that there is no pronounced "peak" pullout resistance during the initial loading cycle. The magnitude of the displacement was selected to be greater than the rib spacing so that the passive resistance due to the inclusion of the ribs was fully mobilized. Note that the shearing resistance includes the friction between the top plate and the bar. This component of the total pullout resistance may be subtracted out using equation (1).

6.0 CONCLUSIONS

The research program objectives for this funding period, as discussed in Sections 1.0 and 2.0 have been met. A computer visualization system has now been established at the University of Michigan and a large Half-Axisymmetric Testing System has been designed and constructed. Pilot tests have been performed which have confirmed system integrity. "Production" testing of the macro- and micro-mechanics of rigid ribbed inclusions in soil will now utilize the computer visualization system to track particle motions around the inclusions. The data thus collected will be used to correlate axisymmetric behavior to previously collected information on particle behavior in plane strain. The analysis of the plane strain behavior was also completed as part of the present research program.

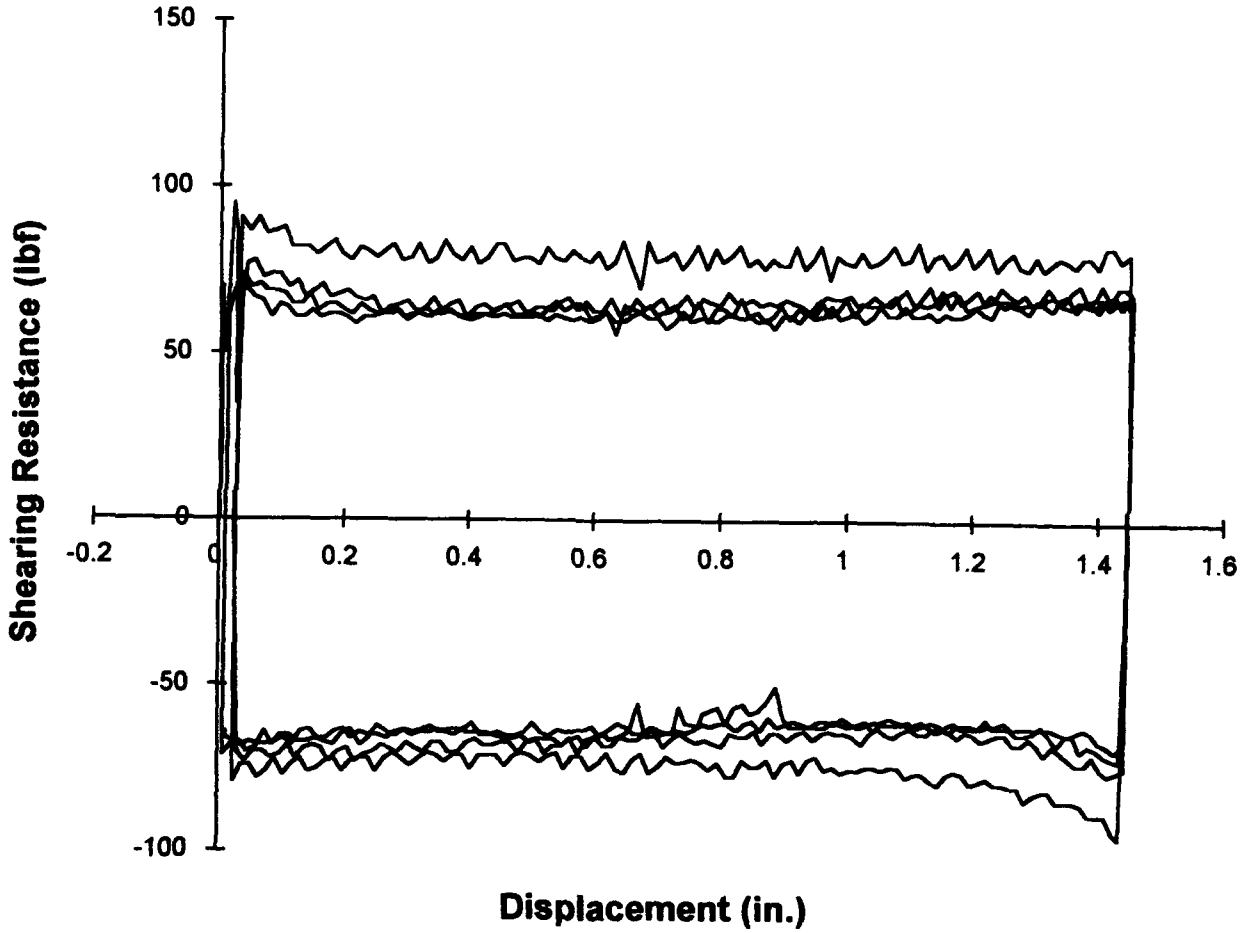

Fig. 9. Load-displacement test results for smooth inclusion at 10 psi in loose Ottawa 20-30 sand.

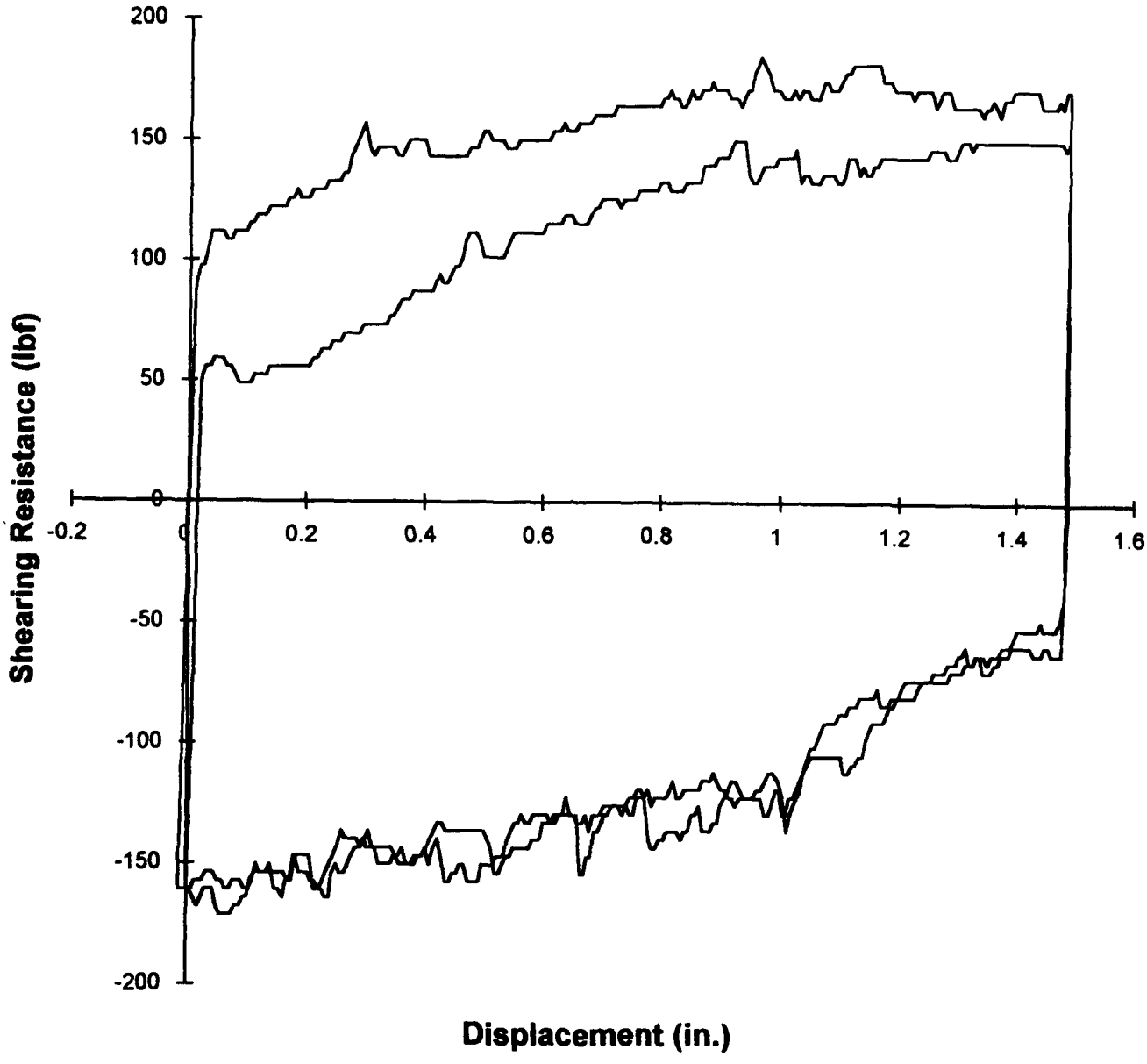

Fig. 10. Load-displacement test results for ribbed inclusion at 10 psi in loose Ottawa 20-30 sand.

7.0 PUBLICATIONS STEMMING FROM THE RESEARCH PROGRAM

Hryciw, R. D. and Irsyam, I. (1993) "Behavior of Sand Particles Around Rigid Ribbed Inclusions During Shear" Soils and Foundations, the Journal of the Japanese Society of Soil Mechanics and Foundation Engineering Vol. 33 No. 3 pp. 1-13.

Raschke, S. A. and Hryciw, R. D. (1994) "Experimental Micromechanics of Geomaterials Through Computer Visualization" Proceedings of the Workshop on Mechanics and Statistical Physics of Particulate Materials held at La Jolla, CA.

Raschke, S. A. and Hryciw, R. D. (1994) "Computer Vision System for Experimental Geotechnics", to be submitted to the ASTM Geotechnical Testing Journal.

Hryciw, R.D. and Raschke, S.A. (1994) "Macro and Micro Mechanics of Soil-Ribbed Inclusion Interaction", to be submitted to the ASCE Journal of the Geotechnical Engineering Division.

8.0 COLLABORATIVE EFFORTS

A collaborative research effort is ongoing with the U.S. Army Waterways Experiment Station (WES) in Vicksburg, MS. Dr. John Peters and Mr. David Horner of the Corps are developing a numerical model for soil behavior which is somewhat different from traditional discrete element models in that the behavior of a cluster of particles is represented by the motions of a single "tracer particle". The model is based on fundamental principles of motion with less emphasis on traditional contact mechanics. The work is being performed on a CRAY supercomputer at WES. The University of Michigan has been working with the WES group by providing experimental data (including visual data) for calibration of the WES model. The WES group in turn provides numerical simulation of the physical experiments conducted at Michigan.

REFERENCES

Donohoe, G. (1992) **The Particle Tracker User's Manual**, Department of Electrical and Computer Engineering, The University of New Mexico, Albuquerque, NM.

Gonzalez, R.C. and Woods, R.E. (1992) **Digital Image Processing**, Addison-Wesley Publishing Company, New York.

Irsyam, M. (1991) "The Mechanical Interaction between Cohesionless Soil and Ribbed Inclusions," a dissertation submitted in partial fulfillment of the requirements for the degree of Doctor of Philosophy (Civil Engineering), The University of Michigan, Ann Arbor, MI.

Tran, H.V. (1993) "Video Particle Tracker for Soil Analysis", a thesis submitted in partial fulfillment of the requirements for the Degree of Master of Science in Electrical Engineering, The University of New Mexico, Albuquerque, NM.

Table 1. Example data file for a sequence tracking four particles over four video frames.

Particle Number	Frame Number	X Coordinate (pixels)	Y Coordinate (pixels)	Minor-Axis (radians)	Major Axis (radians)
Particle 1	1	55	74	-0.254995	1.315802
	2	56	77	-0.233405	1.337392
	3	55	80	-0.273548	1.297248
	4	55	83	-0.179508	1.391289
Particle 2	1	96	121	-0.301211	1.269585
	2	97	124	-0.264087	1.306709
	3	96	127	-0.281305	1.289491
	4	96	130	-0.264500	1.306297
Particle 3	1	169	96	0.047867	1.618663
	2	169	100	0.070597	1.641394
	3	169	103	0.073771	1.644568
	4	169	106	0.058385	1.629181
Particle 4	1	144	107	-0.029829	1.540968
	2	145	110	0.033814	1.604611
	3	144	113	-0.043832	1.526964
	4	145	117	-0.048963	1.521834

SOILS AND FOUNDATIONS Vol. 33, No. 3, 1-13, Sept. 1993
Japanese Society of Soil Mechanics and Foundation Engineering

BEHAVIOR OF SAND PARTICLES AROUND RIGID RIBBED INCLUSIONS DURING SHEAR

ROMAN D. HRYCIW[i] and MASYHUR IRSYAM[ii]

ABSTRACT

The behavior of cohesionless soil around rigid plane ribbed inclusions during shear was investigated. The experimental program included monitoring of individual sand grain movements during plane strain shearing and mapping of zones of dilation, contraction and maximum shear strain. The parameters of study included rib geometry and spacing, soil density, grain shape, grain size and number of shearing cycles. The rib spacing proved to be a particularly important parameter as it controlled the development or lack of development of a passive soil zone ahead of an advancing rib. The initial soil density determined the volumetric straining and the peak load transfer. Beyond the first half-cycle of shearing, both dense and loose sands exhibited similar behavior. Carbowax solidification techniques were also employed to characterize the failure surfaces and to determine localized changes in void ratio in the intrarib region.

Key words: interface shear, ribbed inclusions, sand, shear zones, soil fabric, soil reinforcement (IGC: D6)

INTRODUCTION

The design of reinforced earth and other systems where soil-inclusion interactions dictate engineering behavior is typically based on macroscopically measured loads transferred between the soil and the reinforcement-inclusions. However, the underlying micromechanistic load transfer mechanisms in such systems have not been explored to date and are not fully understood. The study of these mechanisms could greatly enhance the design of soil reinforcement for optimal transfer of loads.

The primary vehicle for study of the load transfer mechanisms around ribbed inclusions is visual observation of individual grain movements during shear. The development of peak loads can be better understood through mapping of zones of dilation, contraction and shear. The stabilization of the transferred loads at post-peak, steady state values is explained by the development of shear bands and passive soil zones ahead of the advancing ribs.

By observing and measuring particle displacements during shear against flat metal surfaces of varying roughness, Yoshimi and

[i] Associate Professor, Dept. of Civil and Environmental Engineering, University of Michigan, 2366 G.G. Brown Building, Ann Arbor, Michigan 48109-2125, USA.
[ii] Graduate Student, ditto.
Manuscript was received for review on October 23, 1992.
Written discussions on this paper should be submitted before April 1, 1994 to the Japanese Society of Soil Mechanics and Foundation Engineering, Sugayama Bldg. 4 F, Kanda Awaji-cho 2-23, Chiyoda-ku, Tokyo 101, Japan. Upon request the closing date may be extended one month.

Kishida (1981), Uesugi and Kishida (1986a, 1986b) and Uesugi et al. (1988) made important contributions to the understanding of the behavior of sand particles at sand-metal interfaces. These studies showed that sand type (shape, constituent minerals, surface roughness), soil density and the metal surface roughness (relative to the soil's D_{50}) are influential factors while soil gradation and normal stress are less important.

The presence of ribs on the inclusion surfaces, such as in reinforced earth ties, conduces additional influential factors. These additional factors include rib geometry, rib spacing and the number of shearing cycles. It was also expected that the ribs would give rise to entirely different load transfer mechanisms than have been observed for flat surfaces. A study of the behavior of sand particles around rigid ribbed inclusions was thus undertaken. The primary factors that were analyzed in the study included sand density, grain shape, rib spacing, rib geometry and number of cycles of shearing. The present paper documents the findings of this observational study. Related works by Irsyam and Hryciw (1991) and Irsyam and Hryciw (1993) present analytical solutions for the pullout resistances of planar and cylindrical ribbed inclusions in sand.

EXPERIMENTAL CONFIGURATION

A direct shear box with dimensions 267 mm × 140 mm × 76 mm as shown in Fig. 1 was constructed with plexiglass walls to facilitate visual observation of grain movements during testing. Various interchangeable ribbed inclusions (Fig. 2) were installed in the central portion of a rigid base plate. A video camera was used to view an enlargement of the intrarib zone on a large monitor. Sand grains were colored to allow the movement of select individual grains to be followed during a test.

In addition to optical monitoring of individual grains, a carbowax solidification technique was developed for identifying shear surfaces. Details of this procedure were presented by Irsyam and Hryciw (1991).

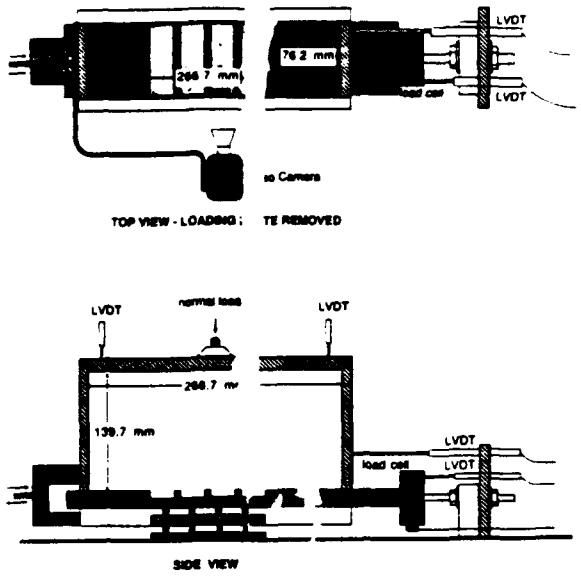

Fig. 1. Experimental configuration for testing ribbed inclusions (from Irsyam and Hryciw, 1991)

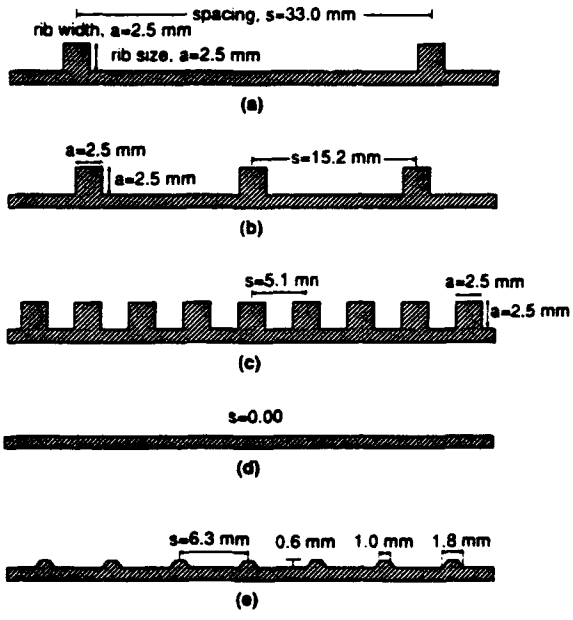

Fig. 2. Rib spacings and geometries tested

COMPUTATION OF INCREMENTAL STRAINS

The monitoring of movements of individual grains enabled the determination of linear and volumetric strain increments. In Fig. 3, δX_i

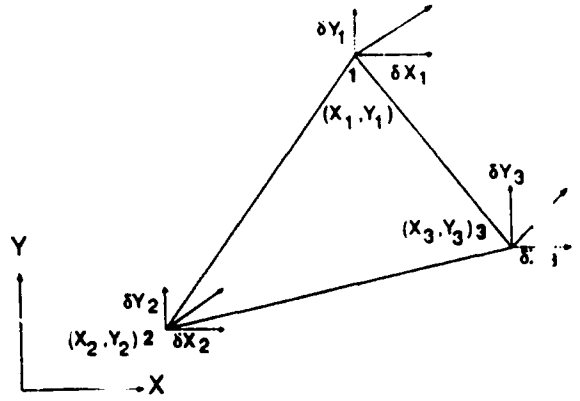

Fig. 3. Triangular mesh for computing strain

and δY_i are the incremental displacements in the X and Y directions of a discrete sand grain located at point i. The displacements of three colored sand grains forming the corners of a triangular mesh element (Fig. 3) defined the strain increments $\delta\varepsilon_x$, $\delta\varepsilon_y$ and $\delta\varepsilon_{xy}$ for the element. The maximum shear strain increment, δ_γ, and the volumetric strain increment δV were then calculated as:

$$\delta_\gamma = \sqrt{(\delta\varepsilon_x - \delta\varepsilon_y)^2 + 4\delta\varepsilon_{xy}^2} = |\delta\varepsilon_1 - \delta\varepsilon_3| \quad (1)$$

and

$$\delta V = \delta\varepsilon_x + \delta\varepsilon_y = \delta\varepsilon_1 + \delta\varepsilon_3 \quad (2)$$

where $\delta\varepsilon_1$ and $\delta\varepsilon_3$ are the increments of major and minor principal strain respectively.

Zones of relatively high contraction, dilation and shear strain increment could then be mapped. These zones were defined as the areas in which either the dilation, contraction or maximum shear strain increment was distinctly higher than in the surrounding regions.

SOIL DESCRIPTION

The soils used in the experiments were Ottawa 20-30 and Glazier Way 20-30 sands. Both sands are uniform with coefficients of uniformity of 1.3 and 1.1 respectively. However, the Ottawa 20-30 has rounded grains while the Glazier Way sand is angular. The specific gravities of both soils ranged between 2.65 and 2.66. For the Ottawa 20-30, initial void ratios, e_0, of 0.51-0.53, corresponding to relative densities of 90-100% were used to represent dense conditions, while e_0 of 0.62-0.64, corresponding to relative densities of 30%-40% represented the loose condition. For the Glazier Way 20-30, an e_0 of 0.58-0.61 was used, corresponding to relative densities in the range 85%-95% for the dense condition.

Dense samples were prepared by raining the sand into the direct shear apparatus. Different relative densities could be achieved by varying the height of drop. Loose samples were prepared by deposition through a funnel while maintaining the height of drop at essentially zero. All test were performed at applied normal stresses, σ_n, of 15.5 kPa or 50 kPa.

SOIL DENSITY EFFECTS

Results from tests conducted on square ribs with a 33 mm rib spacing (Fig. 2(a)) and Ottawa 20-30 sand are presented in Figs. 4 to 6. Fig. 4 shows typical plots of shear resistance versus relative displacement for loose and dense sand conditions. In this figure subscripts d, l, and r indicate dense, loose, and reversal conditions. Fig. 5 shows grain movements of four increments of forward relative displacement for dense sand (0.0 to 2.0 mm; 2.0 to 4.6 mm; 4.6 to 7.1 mm and 22.9 to 25.4 mm) and Fig. 6 shows grain movements of four in-

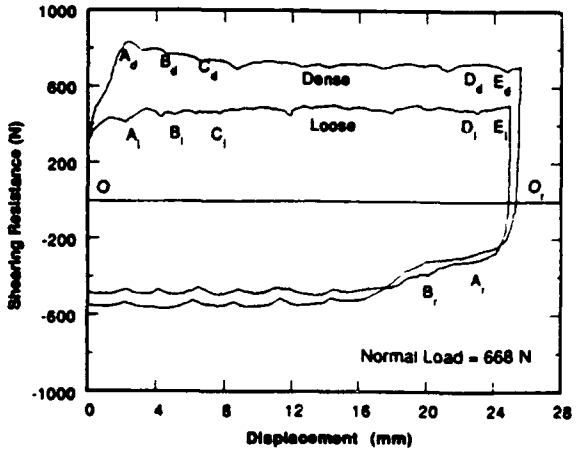

Fig. 4. Typical shear resistance versus displacement for dense (e=0.52) and loose (e=0.63) Ottawa 20-30 sand (a=2.5 mm; s=33.0 mm)

crements of forward relative displacement for loose sand (0.0 to 2.5 mm; 2.5 to 5.1 mm; 5.1 to 7.6 mm and 22.9 to 25.4 mm).

Dense Sand

Pre-peak Behavior

Several important observations could be made concerning changes in soil fabric during the pre-peak stage (Fig. 4, O to A_d, and Fig. 5(a)). During approximately the first 0.25 mm of relative displacement, a relatively high shearing stiffness is observed, during which time intergranular shear stresses develop. When shearing begins, some grains will be pushed into new positions with little difficulty. The normal stresses acting in the direction of movement will be small but the grains will eventually take up positions which will make further sliding more difficult. Other grains will be in an arrangement with the surrounding grains such that it is difficult, or impossible, for them to slide and therefore they move along with the adjacent grains without sliding. After some movement, frictional resistance in the former grains are built up gradually as the grains become impeded in their progress, whereas the latter grains encounter resistance immediately. Therefore, frictional resistance in the aggregate is built up gradually and consists of setting up normal stresses in the grain structure as the grains push or slide along (Cornforth, 1964). Because the structural packing of the grains is dense, the number of grain contacts will be relatively high. As a result, the frictional resistance will be higher for dense than for loose sand.

While the frictional resistance builds up and the grains push or slide along, various magnitudes of interparticle forces are generated at points of contact within the assembly. Continuous shear will alter the equilibrium condition therefore prompting the grains to slide into new positions of equilibrium in directions offering the least resistance to shear. Because of its dense packing, the least resistance to shear is achieved through dilation (volume expansion). The dilation can clearly be seen in Fig. 5(a). Significant movements of sand grains occur along the entire region captured by the camera. The sand particles move not only tangc tially to the plate, but also in the upward ormal direction. A zone of relatively high lation occurs above the inclusion surface. Ti : direction of the grain movements gradually aries from 0 degree from the horizontal at t e interface to 50 degree from the horizontal about 6 mm above the rib.

As mentioned earlier, fricti ial resistance in the aggregate is built up grac ially and consists of setting up normal stre s in the grain structure as the grains push slide along. However, sliding allows the gr structure to loosen or dilate in dense soil, ..h in turn reduces dilation induced normal stresses. These two factors; the more sliding required to mobilize the shearing resistance, the less resistance can be mobilized, result in a peak shear stress (Cornforth; 1964). The peak shear stress was observed at 2.0 mm of relative displacement or at point A_d in Fig. 4.

The peak shear stress may also result in a zone of relatively high shear strain increment associated with failure initiation. Because of the rib's rigid boundary, the failure initiates just above the rib as can be seen in Fig. 5(b). The zone may represent a region in which shear stresses along the grain contacts have already reached limiting equilibrium. Therefore, slight displacement of the plate results in loss of equilibrium among the grains. This relatively high shear deformation is not the cause of failure initiation at the peak, as assumed by Coulomb, but is the later result of the failure (Rowe 1962).

Post-Peak Behavior

Continued shearing beyond the peak stress results in continuous loosening of dilatant soil. As a result, in order to maintain the stress equilibrium with the external stresses during shearing, new positions of equilibrium in directions offering the least resistance to shear can be achieved using less energy in dilation. Therefore, the shearing resistance decreases with the increase of displacement as can be seen from point A_d to C_d in Fig. 4.

The rearrangement of the particle assembly along the shear zone to new positions of equilibrium will narrow the shear zone. As can

be seen in Figs. 5(b) and 5(c) the shear zone thickness changes gradually and grain deformations gradually become localized into a narrower zone during the course of post-peak deformation. At the same time, the zone of limiting equilibrium expands to the front and back of the rib and results in a longer zone of relatively high shear strain increment. This can be viewed as failure surface formation. Grain rearrangement in this zone is already in the post dilation stage, hence, the zone of relatively high dilation moves away from the rib.

The decrease in shearing resistance continues until a complete failure surface is formed. Although the entire zone between adjacent ribs could not be captured optically, carbowax solidification tests, as will be discussed subsequently, indicate that for this rib spacing, a curved failure surface initiates above the tops of the rib, touches the base plate and continues to the rear face of the next rib. The complete formation of a failure surface may be associated with the establishment of constant residual shear resistance. Several experimental results indicated that the residual shear resistance stabilizes at 13 to 20 mm of relative displacement as can be seen in the Fig. 4. It was also observed that the displacement required to establish the residual shear stress depends on the rib spacing as will be subsequently discussed.

The constant residual shear resistance is attributed to the full formation and mobilization of passive resistance on the front of the rib as can be seen in Fig. 5(d). In addition to the passive resistance, the residual shear resistance also consists of friction between the soil and the base of the inclusion in the intrarib region. Extensive discussion about the load transfer mechanism and its analytical solution for this stage can be found in Irsyam and Hryciw (1991).

In the residual stage, grain deformations are concentrated in a 2.5 rib height thick shear zone. This stage can be envisaged as one in which part of the particles are effectively resisting the applied shear and just about to break contact while other particles which are at limiting equilibrium, have failed and are making new contacts (Rowe, 1962). In this stage grains may displace each other under the applied stresses without any net volume change. It is expected that a critical void ratio is developing at the front and a loose fabric is developing at the back of the rib.

Although measurements of vertical displacement at the top of the soil mass reflect the overall volume change of the sample, these readings do not reflect the actual density changes in the shear zone between the ribs. Therefore, a carbowax impregnation technique for determining void ratio distribution in the intrarib region was adopted (Hryciw and Irsyam, 1990). The carbowax impregnation results can be seen in Fig. 7. They show that the void ratio between the ribs varies from a critical void ratio on the front to a loose fabric at the back of the ribs.

Loose Sand

Several important observations could be made concerning changes in soil fabric for loose sand as can be seen in Fig. 4 and Fig. 6. During approximately the first 0.25 mm of relative displacement, similarly to the dense condition, a relatively high shearing stiffness is observed, during which time the intergranular shear stresses are developing. Additional displacement of the ribbed plate rearranges and locates sand particles into new positions of equilibrium in a direction offering the least resistance to shear. Because the structural packing of the grains is loose, the least

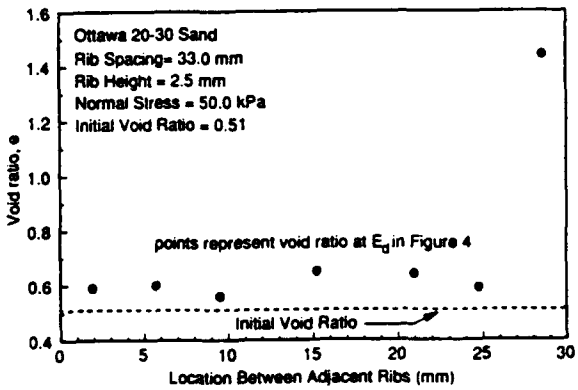

Fig. 7. Void ratio in the intrarib region before and after shearing (Ottawa 20–30; $e=0.52$ $\sigma_n=50.0$ kPa; $a=2.5$ mm; $s=33.0$ mm)

resistance to shear is achieved t' ough contraction as shown in Figs. 6(a) and (b). A zone of relatively high contraction is f· ınd in front of the rib.

This contraction will increas the number of grain contacts and frictional resistance will build up as the grains push oı ılide along. As the grains slide into new pc itions, further sliding becomes more difficult Unlike dilation in dense sand, contraction c es not require energy to be spent. As a re ılt, loose sand does not exhibit dilation : duced normal stress. Hence, loose sand requ s less shearing resistance and reaches its n . ·num shear stress without passing a previo.s ,eak (from O to C_1 in Fig. 4).

As in dense sand, continuous shearing will gradually change the void .atio and the thickness of the shear zone, localize grain deformations, and form a failure surface as shown in Figs. 6(a), 6(b), and 6(c). The process continues until, after considerable displacement, a failure surface is completely formed. The shear zone is localized at about 2.5 rib heights, and a constant residual shear stress develops. Several direct shear test results on this rib spacing indicate that complete formation of a failure surface is observed at about 11.0–18.0 mm of displacement. This constant shear stress once again consists of full mobilization of passive resistance on the rib front (Fig. 6(d)) and soil-metal friction in the intrarib region. An assessment of the relative contributions of passive and friction resistance can be found in Irsyam and Hryciw (1991).

Compared to dense sand, Fig. 6(d) suggests that loose sand exhibits a smaller passive zone at the front of the ribs. This behavior was confirmed by carbowax solidification on Ottawa and Glazier Way sand shown in Fig. 8. For Ottawa 20–30, the height of the passive wall, AB, was 2.0 rib heights for dense and 1.8 rib heights for loose sand. This suggests that the initial void ratio effect has not yet been eliminated during the first 25 mm of forward relative displacement.

After the constant shear resistance is established the behavior of both dense and loose sand is basically very similar as can be seen by comparing Fig. 5(d) with Fig. 6(d). Irsyam and Hryciw (1991) have modelled the intrarib zones as shown in Fig. 9. They found that the optimum rib spacing is one which allows a full passive zone to develop yet keeps the length of the transition zone to a minimum. In both dense and loose sands, during continuous post-peak shearing the grains within the moving passive zone will continually adjust into their critical void ratio, while the grains behind the advancing rib become loose. A compressive soil arch develops between the top of the rib and the base plate as shown in Fig. 9.

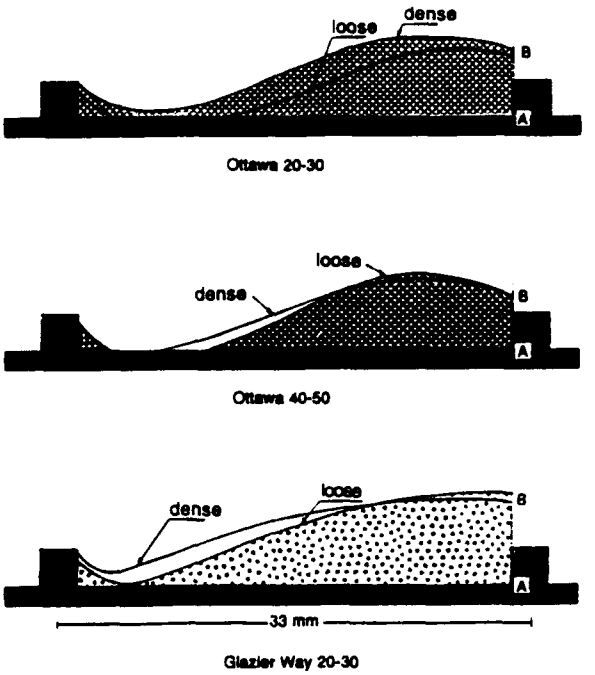

Fig. 8. Density effects observed from carbowax solidification (Ottawa 20–30; $a=2.5$ mm; $s=33.0$ mm)

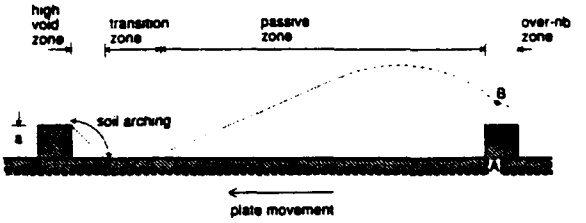

Fig. 9. Intrarib zones for large rib spacings

EF :CT OF SHEARING REVERSAL AND SU SEQUENT CYCLES

: g. 10 shows grain movements of two incre ients of reverse displacement (25.4 to 22.9 mn and 22.9 to 20.3 mm) for dense sand. Th :e increments correspond to points O_r to A_r nd A_r to B_r in Fig. 4.

: is noted that the peak stress exhibited during he first half-cycle was not observed during re rse displacement. Sixteen other direct she r tests on dense sand performed by the aut rs confirmed that during all subsequent cyc only the residual shear resistance develops. A typical cyclic load deformation curve for the dense sand is shown in Fig. 11. Basically, the behavior of both dense and loo sand is very similar after constant shear resistance is established on the first cycle. The difference between the shear resistance for loose and dense soil upon reversal of the shearing direction and upon subsequent cycles was not significant as can be seen in Fig. 4. It suggests that the final void ratio distribution that develops throughout the shear zone is independent of the initial void ratio.

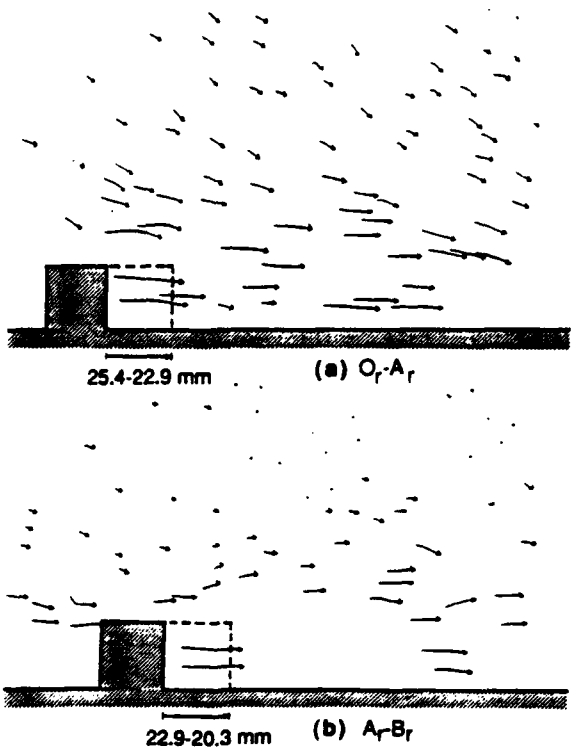

Fig. 10. Displacements of select grains upon shear reversal (Ottawa 20-30; $e=0.52$ $\sigma_n=50.0$ kPa; $a=2.5$ mm; $s=33.0$ mm)

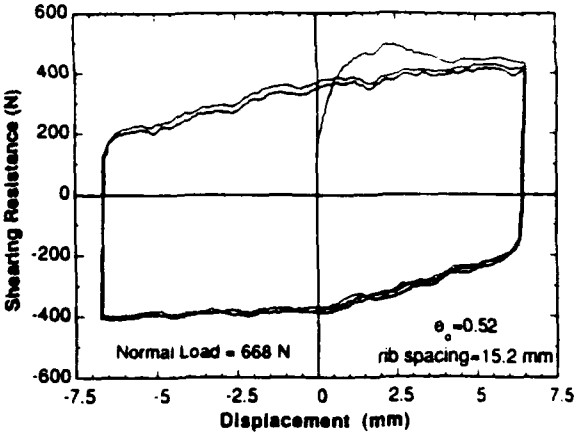

Fig. 11. Typical cyclic load-displacement test result (Ottawa 20-30; $e=0.52$ $\sigma_n=50.0$ kPa; $a=2.5$ mm; $s=15.2$ mm)

After only one rib spacing of relative displacement in the forward direction, the soil fabric at the front of the rib reaches its critical void ratio, on the other hand, the grain structure at the back of the rib becomes loose. If shearing is reversed, the rib will face the loose fabric that was initially behind an advancing rib. As a result, it can be expected that the initial shear resistance and the grain behavior will be similar to that of loose sand. As shown in Fig. 10(a), the least resistance to shear will be achieved through contraction. This contraction will increase grain contacts and build up frictional resistance as the grains push or slide along (point O_r to A_r in Fig. 4).

Fig. 4 also shows that during reverse motion, shearing resistance continues to build from 25 mm (O_r) all the way to 16 mm. This phenomena may be attributed to the fact that the denser grain structure that constituted the passive zone during forward displacement is now at the back of a rib and therefore greater displacement is required before intergranular stresses build up in this region.

RIB SPACING AND GEOMETRY EFFECTS

Rib Spacing

In addition to the 33 mm rib spacing, 25.2

mm (Fig. 2(b)) and 5.1 mm (Fig. 2(c)) spacings were also studied. The results for the 25.2 mm spacing and dense sand are presented in Fig. 12. The figure shows grain movements at three increments of relative displacement; 0 to 2.5 mm and 2.5 to 5.1 mm for the pre-peak state and 22.9 to 25.4 mm for the residual state.

Similarly as for the large spacing during the pre-peak stage, significant movement of sand grains occurs along the entire sample as shown in Figs. 12(a) and 12(b). The sand particles move not only in the tangential but also in the upward normal direction and result in volume expansion or dilation.

For the 25.2 mm rib spacing, part of the grains between adjacent ribs are trapped and move as a unit with the ribbed plate. These trapped grains will significantly reduce the height of the soil wall that pushes on the passive zone. Therefore, large grain movements are confined to a narrower zone. In addition, a constant shear resistance develops sooner because less displacement is required to fully develop the failure surface.

As can be seen in Fig. 12(c), from optical monitoring and Fig. 13 from carbowax solidification, a wavy shear surface was observed to ultimately develop which could be characterized as having a wavelength of one rib spacing, peaks midpoints between adjacent ribs and troughs bottoming several grain diameters above the front face of each rib. Unlike for the 33 mm spacing, a shear surface fails to dip below the tops of the ribs and scrape the base of the plate. As a result, a full passive zone fails to develop and the constant shear resistance will be primarily due to soil-soil friction with some contribution from a partially developed passive zone.

For the 5.1 mm rib spacing, all passive resistance disappears. In this case, the ribbed plate behaves merely as a rough surface and the pullout resistance becomes partially due to soil-soil friction and partially due to friction between the soil and the tops of the ribs.

Rib Geometry

In order to understand the effect of rib geometry on particle behavior, a trapezoidal rib was also tested (Fig. 2(e)). This rib size and spacing is typical of that found on a #3 (9.5

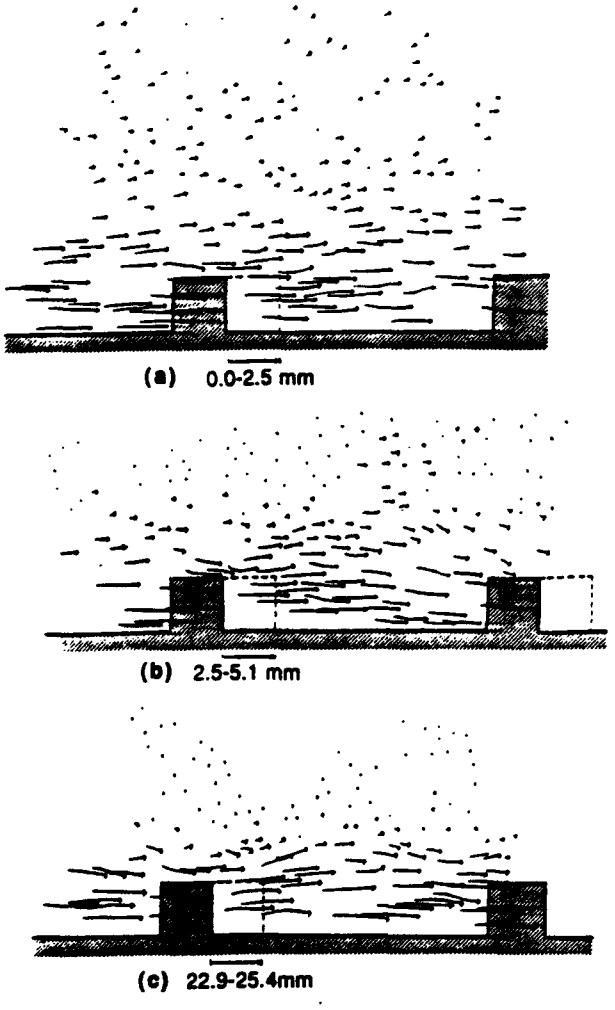

Fig. 12. Displacements of select grains (Ottawa 20–30; $e=0.52$ $\sigma_n=15.5$ kPa; $a=2.5$ mm; $s=15.2$ mm)

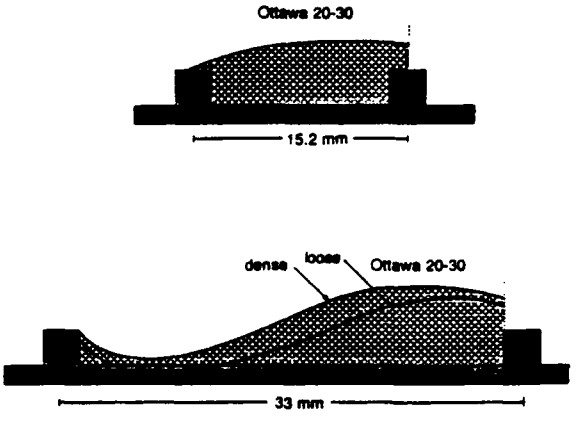

Fig. 13. Rib spacing effects on failure surface from carbowax solidification (Ottawa 20–30; $a=2.5$ mm)

mm diameter) reinforcing rod. Several increments of relative displacement were observed, however, only two increments of relative displacement, 0 to 3.2 mm and 12.7 to 15.9 mm, are presented in Fig. 14 as they adequately represent the behavior.

As can be seen in Fig. 14, no passive zone (as was observed for the square) rib can develop for this rib geometry. Compared with the square rib, grain deformations are observed in a narrower zone during the pre-peak and residual states. The geometry of the rib and the surface roughness of the plate allow grains to override from the front to the back of the rib. Hence, the ribbed plate behaves merely as a rough surface. Therefore, the shear resistance becomes purely due to soil-soil friction and its value may approach the shear strength of soil.

Roscoe (1970) states that the shear zone thickness is a small multiple of the mean grain size. This means that the thickness is not affected by any geometrical dimensions of a soil body other than its grain size (Mulhaus and Vardoulakis, 1987). Figs. 14(a) and 14(b) show that the shear zone thickness varies from about 6.5 mm (12 grain diameters) during the first 3 mm of relative displacement to about 3.3 mm (6 grain diameters) at the residual state. For the residual state, the 6 grain diameters are in a good agreement with previous investigations that studied the behavior of sand on a rough surface and the shear zone thickness within the soil body (Table 1). However, carbowax solidification tests showed that Ottawa 20–30 and Ottawa 40–50 yield the same shear zone thickness of 3.3 mm. This suggests that the geometry of the ribs also influences the shear zone thickness.

Smooth Plates

The grain displacements of tracked particles on a smooth aluminium plate, without ribs, for both dense and loose Ottawa 20–30 sand are presented in Fig. 15. The behavior is very

Table 1. Observed shear zone thicknesses

Study	Shear Zone Thickness / Grain Diameter	Test Type
Present study	≈6	Plane strain
Uesugi et al. (1988)	3–4	Friction Test
Yoshimi and Kishida (1981)	5–8	Friction Test
Roscoe (1970)	≈10	Simple Shear
Cornforth (1964)	6–20	Plane Strain
Vardoulakis et al. (1978)	4–6	Plane Strain
Mulhaus and Vardoulakis (1987)	≈8	Cosserat granular medium (plasticity)

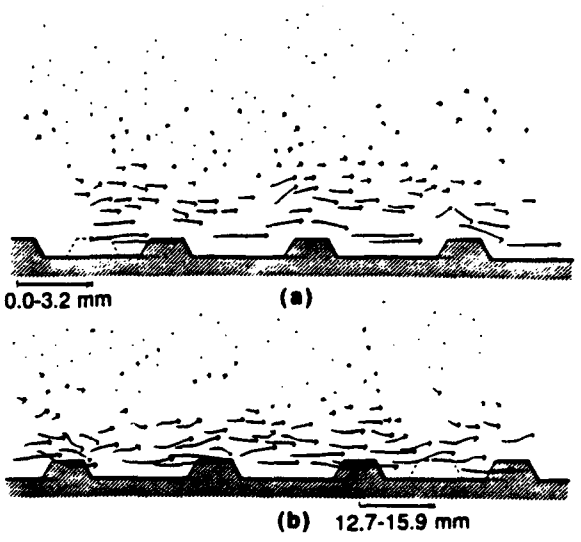

Fig. 14. Displacements of select grains around trapezoidal ribs shown in Fig. 2(e) (Ottawa 20–30; $e=0.52$; $\sigma_n=15.5$ kPa; $s=6.4$ mm)

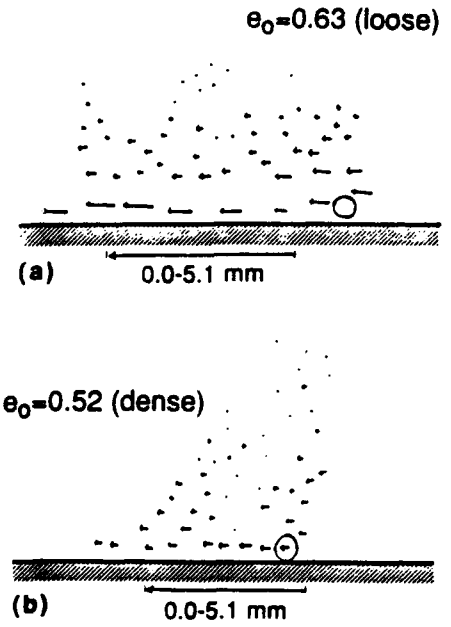

Fig. 15. Displacements of select grains on a smooth plate (Ottawa 20–30; $\sigma_n=15.5$ kPa)

similar to previous results reported by Yoshimi and Kishida (1981) and by Uesugi et al. (1988). As shown in the figure, the sand is sheared uniformly without developing a shear zone. Therefore, the displacement of the interface consists mostly of particles slipping on the metal surface. The interface friction angle may be less than one half of the particle-to-particle friction angle (Yoshimi and Kishida, 1981).

Summary of Rib Effects

With the presence of trapezoidal ribs, the plate behaves as a rough surface. Therefore, shear failure occurs within the sand mass, instead of sliding along the contact surface, and the shear resistance may be related to the shear strength of the soil. With square ribs, a passive zone can develop and it can alter the behavior of particles and significantly increase the shear resistance.

SAND GRAIN SIZE AND SHAPE EFFECTS

Grain Shape Effects

In order to study the effect of grain angularity on particle behavior, a dense angular sand (Glazier Way 20–30) was also tested. The rib geometry used in this visual observation was trapezoidal. The test was conducted using 3 increments of relative displacement: 0 to 3.2 mm, 3.2 to 6.4 mm and 6.4 to 9.5 mm. The results are shown in Fig. 16.

It was expected that angular particles would interlock more thoroughly than rounded particles (Lambe and Whitman, 1979 and Rowe, 1962). In order to reach the residual stage, particles do not only slip but also roll. Rolling of angular particles merely disturbs the equilibrium of neighboring particles, hence angular material has a more notable effect on volume strain, the maximum dilatancy rate is especially prevalent in the dense condition (Frossard, 1979). In addition, the initial packing of the grains is dense where the least resistance to shear is achieved through dilation or volume expansion. Therefore, unlike Ottawa 20–30, significant movements of sand grains were observed throughout the area

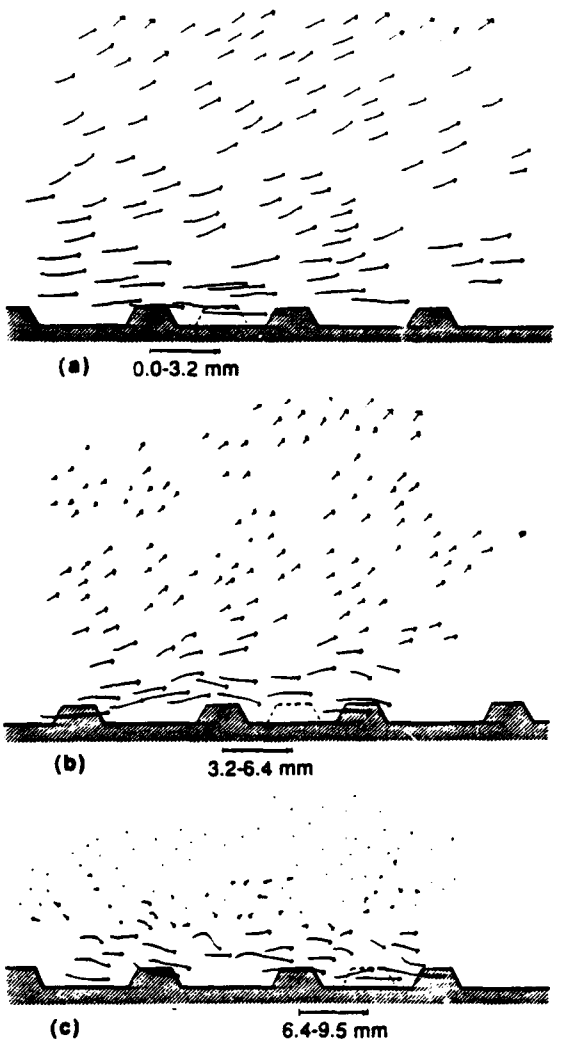

Fig. 16. Displacements of select grains for angular sand. (Glazier Way 20–30; $e=0.48$ $\sigma_n=15.5$ kPa; $a=2.5$ mm; $s=6.4$ mm)

covered by the camera before the residual stage is established (Figs. 16(a) and 16(b)). The movement is not only in the tangential but also in the upward normal direction. The angular material would thus be expected to exhibit a higher shear strength.

After more than one rib spacing of relative displacement (from 6.4 to 9.5 mm), however, Glazier Way 20–30 exhibits very similar behavior to Ottawa 20–30 as can be seen in Fig. 16(c). The grain displacements are confined in a narrow zone of about 3.2 mm (6 grain diameters) thickness with no further volume change. Even the grain displacements are very similar in this stage. Nevertheless, the angular

material may exhibit higher residual shear strength because it still has a higher friction angle in the residual state (Lambe and Whitman, 1968).

In addition to the higher residual shear strength, the carbowax solidification technique using square ribbed inclusions indicated that the higher friction angle may also result in a larger passive zone on the front of the ribs as can be seen in Fig. 17. It can be expected that in order to have a fully developed passive zone, angular particles will require a larger rib spacing.

Grain Size

The measurement of particle displacements using a grain size smaller than Ottawa 20–30 sand may provide important contributions to the understanding of the effect of grain size on the behavior of sand particles around ribbed inclusions. Unfortunately, the authors found that it was very difficult to track the movements of such small grains. The residual failure surfaces could be accessed only by using the carbowax solidification technique.

The results from the carbowax tests using rib spacing equal to 1.3 in are presented in Fig. 18. The results showed the effect of grain size is insignificant to the failure surface. It may suggest that the distance AB, the height of the soil contributing to the passive wall, is more controlled by the rib size and rib roughness rather than by grain size. Fig. 18 also showed

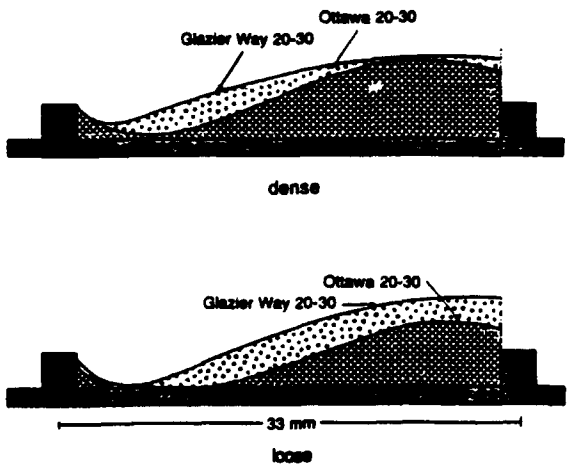

Fig. 17. Grain shape effects on failure surface from carbowax solidification (a=2.5 mm; s=33.0 mm)

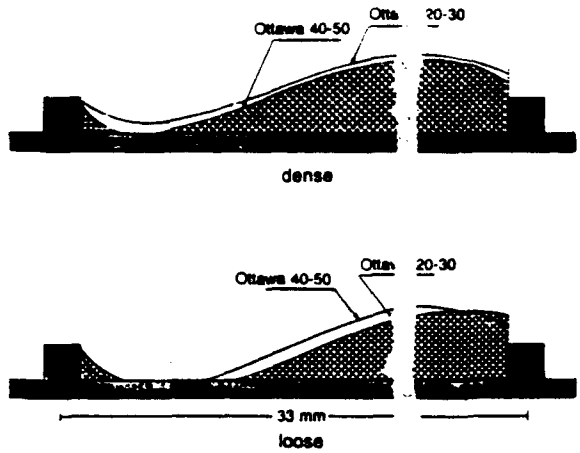

Fig. 18. Grain size effects, on failure surface from carbowax solidification (a=2.5 mm; s=33.0 mm)

that the failure surfaces of dense and loose Ottawa 40–50 are more similar to those of dense and loose Ottawa 20–30. It suggests that for the same amount of displacement, smaller grains will have less initial void ratio effect. In other words, the amount of plate movement required to reach a critical state may be related to the grain size.

SUMMARY AND CONCLUSIONS

An experimental investigation of the behavior of sand particles around rigid ribbed inclusions has been performed. The tests were performed in a plexiglass walled direct shear device. This allowed the movements of individual sand grains to be followed during shear. Zones of relatively high contraction, dilation and shear strain increment were mapped. In dense sand, dilation, followed by progressive formation of a shear surface was observed and related to the development of peak and residual strengths. In loose sands, contraction was clearly in evidence and no peak behavior was discerned. Upon reversal of the shearing direction, and on all subsequent shearing cycles, both initially dense and loose sands displayed similar behavior and similar shearing resistance thereby confirming the establishment of a critical void ratio.

Carbowax solidification techniques were used to determine the shapes of the shear surfaces and to establish the void ratios in the in-

trarib region. In general, there was excellent agreement between the carbowax test results and visual observations.

Tests were also conducted to investigate the effects of rib spacing, rib geometry, grain size and grain shape. While full passive zones developed for the 33 mm rib spacing, at a 25.2 mm spacing grains were trapped between the ribs and only a partial passive zone could develop. Previous studies have shown that the pullout resistance is highest when the number of full passive zones per length of inclusion is maximized.

Small, closely spaced trapezoidal ribs such as found on reinforcing rods were incapable of producing a passive zone. However, a shear zone was observed to develop through the sand above the ribs. By contrast, no shear zone whatsoever was observed for smooth plates. The grains essentially slipped along the rib-less surface during shear.

Angular sands displayed greater movement than rounded sands prior to residual strength development and the passive zone was generally larger. Ottawa 20–30 and Ottawa 40–50 sands displayed very similar behavior.

ACKNOWLEDGEMENTS

This study was part of a research program supported and funded by the United States Air Force office of Scientific Research under Grant No. AFOSR-88-0166 and F49620-92-J-0216 Financial support for Mr. Irsyam's graduate studies was partially provided by IUC-ITB/MUCIA-World Bank XVII.

REFERENCES

1) Cornforth, D. H., (1964) "Some experiments on the influence of strain conditions on the strength of sa ," Géotechnique, Vol. 14, No. 2, pp. 143–167.
2) Fr sard, A., (1979) "Effects of sand grain shape on in particle friction; indirect measurements by R e's stress dilatancy theory," Géotechnique, Vol. 2 No. 3, pp. 341–350.
3) H sen, Bent (1958) "Line ruptures regarded as narrc rupture zones: basic equations based on k: matic considerations," Conf. Earth Pressure P bl., Brussel 1, 39–49.
4) Ir yam, M. and Hryciw, R. D. (1993) "Friction and p: sive resistance in soil reinforced by cylindrical ri' ed inclusions," tentatively accepted by the Inter- r ional Journal for Numerical and Analytical M thods in Geomechanics.
5) Hryciw, R. D. and Irsyam, M. (1990) "Shear zone char terization in sands by carbowax impregnation , STM Geotechnical Testing Journal, Volume 12, Number 1, pp. 49–52.
6) Irsyam, M. and Hryciw, R. D. (1991) "Friction and passive resistance in soil reinforced by plane ribbed inclusions, Géotechnique, Vol. 41, No. 3.
7) Lambe, T. W. and Whitman, R. V. (1979) Soil Mechanics, John Wiley and Sons, New York.
8) Mulhaus, H. B. and Vardoulakis, I. (1987) "The thickness of shear bands in granular materials," Géotechnique 37, No. 3, pp. 271–283.
9) Roscoe, K. H. (1970) "The influence of strains in soil mechanics," Géotechnique, Vol. 20, No. 2, pp. 129–170.
10) Rowe, P. W. (1962) "The stress dilatancy relation for static equilibrium of an assembly of particles in contact," Proc. Royal Soc. A 269, pp. 500–527.
11) Uesugi, M. and Kishida, H. (1986a) "Influential factors of friction between steel and dry sands," Soils and Foundations, Vol. 26, No. 2, pp. 33–46.
12) Uesugi, M. and Kishida, H. (1986b) "Frictional resistance at yield between dry sand and mild steel," Soils and Foundations, Vol. 26, No. 4, pp. 139–149.
13) Uesugi, M., Kishida, H. and Tsubakihara, Y. (1988) "Behavior of sand particles in sand-steel friction," Soils and Foundations, Vol. 28, No. 1, pp. 107–118.
14) Yoshimi, Y. and Kishida, T. (1981) "Friction between sand and metal surface," Proc. of 10th ICSMFE, Vol. 1, pp. 831–834.
15) Vardoulakis, I., Goldscheider, M. and Gudehus, G. (1978) "Formation of shear bands in sand bodies as a bifurcation problem," International Journal for Numerical and Analytical Methods in Geomechanics, Vol. 2, pp. 99–128.